Journal of Volcanology and Geothermal Research xxx (2010) xxx–xxx

Contents lists available at ScienceDirect

Journal of Volcanology and Geothermal Research

journal homepage: www.elsevier.com/locate/jvolgeores

Rhyolitic phreatomagmatism explored: Tepexitl tuff ring (Eastern Mexican Volcanic Belt)

Allison Austin-Erickson [a,*], Michael H. Ort [a], Gerardo Carrasco-Núñez [b]

[a] Department of Geology, PO Box 4099, Northern Arizona University, Flagstaff, AZ 86011, USA
[b] Centro de Geociencias, Universidad Nacional Autónoma México, Juriquilla, Querétaro., 76230, México

ARTICLE INFO

Article history:
Received 26 February 2010
Accepted 3 September 2010
Available online xxxx

Keywords:
rhyolitic phreatomagmatism
Mexican volcanoes
tuff ring
dome explosion

ABSTRACT

Rhyolitic Tepexitl tuff ring in the Serdán-Oriental Basin of the eastern Trans-Mexican Volcanic Belt is a young, well-preserved circular crater — a simple morphology that belies a more complex eruptive history. Field observations, ash studies (granulometry, componentry, and morphology) and volatile data (LOI and XRF) allow the broad division of the Tepexitl deposits into two sequences: a lower sequence characterized by fine-grained deposits with abundant bomb and lapilli sags, and an upper sequence of coarse-grained deposits that show little to no deformation. The early eruptions at Tepexitl are interpreted to have been dominated by discrete, highly efficient, phreatomagmatic blasts, which caused a progressive deepening of the eruptive center (lower sequence), followed by a transition to dominantly magmatic behavior in the upper sequence. Dome growth occurred at the end of the eruption, but subsequent retrogressive explosions triggered by external water destroyed all trace of the original dome morphology.

Molten fuel-coolant interaction (MFCI) is commonly thought to cause the repetitive water–magma interaction in phreatomagmatic eruptions, but a process by which magma and viscous felsic magmas can mingle prior to explosive interaction has not been described. A viable mechanism for rhyolitic MFCI, based upon field work at Tepexitl and laboratory experiments, requires that fluidized sediments intrude marginal fractures in the rhyolite magma, creating enough interfacial surface area to initiate phreatomagmatic explosions from within the interior of a rising plug or dome.

1. Introduction

Phreatomagmatic explosions are caused by a type of molten fuel-coolant interaction (MFCI) in which magma is the fuel and water the coolant. The highly explosive eruptive dynamics resulting from the direct contact between fuel and coolant have been explored in great detail for mafic melts, through a combination of field observations (e.g. Houghton et al., 1999; Hooten and Ort, 2002), lab experiments (e.g. Büttner et al., 1999, 2002; Dellino et al., 2004; Mastin, 2007), and resultant grain size and shape analysis (e.g. Wohletz, 1983; Büttner et al., 2002), but rhyolitic phreatomagmatic dynamics have not been as closely examined. Field evidence demonstrates that rhyolitic phreatomagmatism occurs (e.g. Sheridan and Updike, 1975; Sieh and Bursik, 1986; Heiken and Wohletz, 1987; Houghton et al., 1987; Sheridan et al., 1987; Heiken et al., 1988; Brooker et al., 1993; Roache et al., 2000, Cano and Carrasco-Núñez, 2008), but rhyolitic phreatomagmatic dynamics have not been described in detail.

MFCI occurs as a four-step process (Morrissey et al., 2000). Coarse mixing, the first step, occurs when the two liquids mingle with a thin vapor film separating them. This stage lasts for seconds to minutes, and leads to the second stage, in which the vapor film collapses and the two liquids hydraulically couple, over a period of milliseconds. Heat transfer increases by an order or two of magnitude (Zimanowski, 1998; Büttner et al., 2002), with the melt cooling and the water heating. The third stage, also milliseconds in length, is the fine fragmentation of the magma. Shock waves exceed the bulk modulus of the magma and cause fronts of brittle failure to move through the magma. Thermal granulation may also finely fragment the magma at this stage. The water then flashes to vapor in the fourth stage, leading to a very rapid expansion and explosion lasting seconds to minutes (Zimanowski, 1998). This MFCI process is well established through experimental and field evidence for water interacting with relatively low-viscosity fluids, such as basalt (10–100 Pa s). It is not clear, however, how a very viscous magma, such as a rhyolite (10^7–10^{10} Pa s), could undergo the coarse mixing phase needed to precipitate the rest of the MFCI process (Zimanowski, 1998).

Tepexitl tuff ring, located at the eastern end of the Trans-Mexican Volcanic Belt (TMVB), has well-preserved deposits and easily accessible crater deposits, not obscured by an inner crater dome, which makes it an excellent location to study the near-vent facies and ash shapes that result from the interaction of rhyolitic magma with external water. Tepexitl is one of a few monogenetic rhyolitic centers

* Corresponding author. 4804 Signal Forest Drive, Signal Mountain, TN 37377, USA.
E-mail addresses: allison.a.erickson@gmail.com (A. Austin-Erickson), michael.ort@nau.edu (M.H. Ort), gerardoc@geociencias.unam.mx (G. Carrasco-Núñez).

0377-0273/$ – see front matter © 2010 Elsevier B.V. All rights reserved.
doi:10.1016/j.jvolgeores.2010.09.007

located on a fault zone through basement limestone in the Serdán-Oriental Basin, where bimodal volcanism has been active from late Pleistocene through Holocene time (Fig. 1; Carrasco-Núñez et al., 2007; Ort and Carrasco-Núñez, 2009). Evidence for water in the eruptive system includes abundant bomb sags, accretionary lapilli, scour channels, undulatory bedding, and iron-rich lithic clasts that have altered surrounding lapilli in-situ (a post-depositional process dependent on water and heat). Tepexitl eruptions were fueled by the same water source as other maars in the area, a shallow sandy aquifer locally termed the Toba Café (Siebe and Verma, 1988; Carrasco-Núñez et al., 2007; Erickson, 2007; Ort and Carrasco-Núñez, 2009). This fine-grained mixture of eolian and fluvial sediment is largely derived from local volcanoes and continues to accumulate in the basin.

In order to evaluate the mechanisms for and consequences of rhyolitic phreatomagmatism at Tepexitl, the eruptive history was assessed (discussed in this paper) and MFCI experiments were conducted with select samples (Austin-Erickson et al., 2008). The conclusions of these studies arise from a detailed examination of the deposits: small-scale changes of grain size distributions, componentry, and ash morphology of the tuff as well as large-scale changes of bulk chemistry, petrography, and textural analyses of juvenile

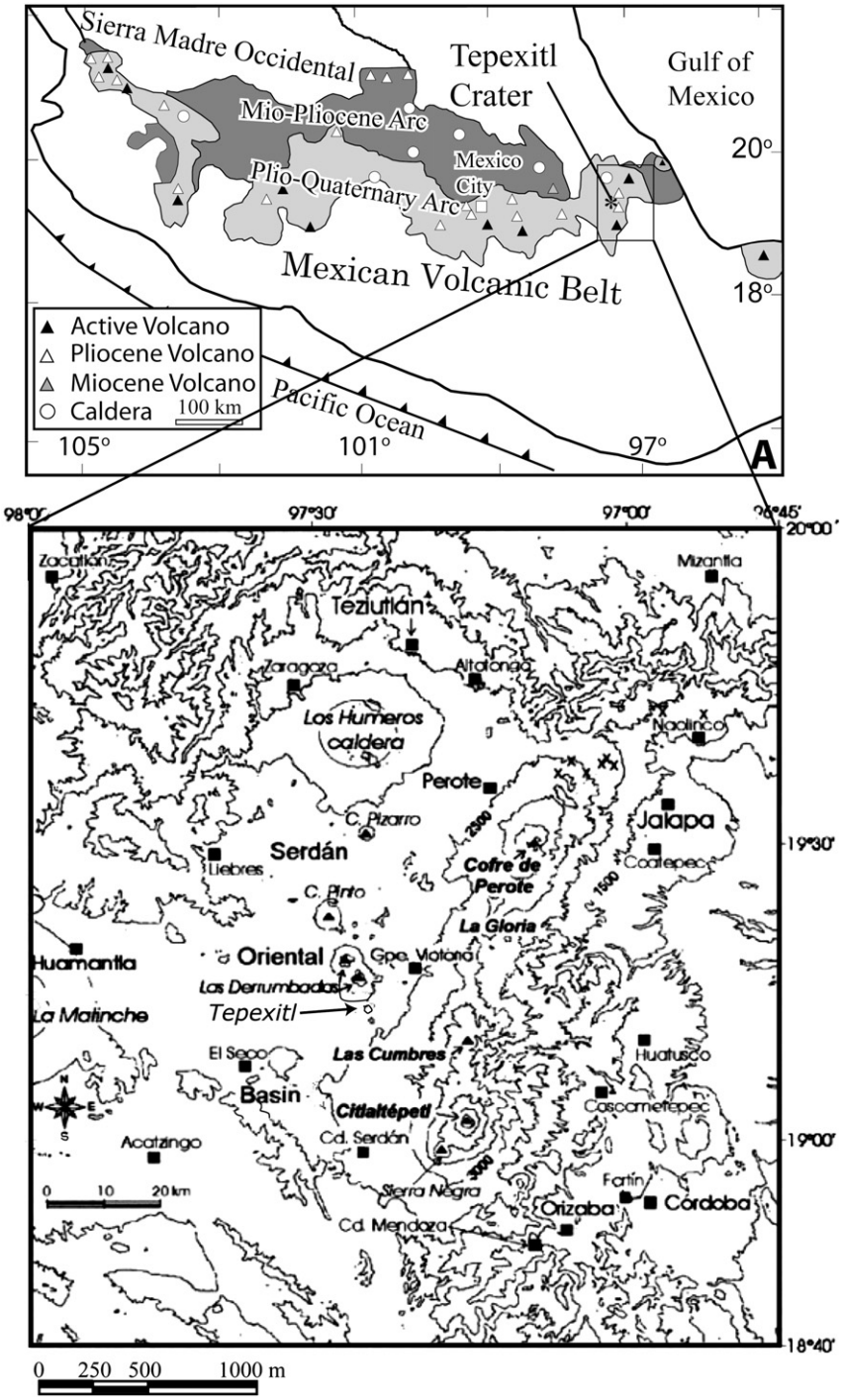

Fig. 1. Location of Tepexitl tuff ring within the Serdán-Oriental Basin, a topographic low near the eastern edge of the Trans-Mexican Volcanic Belt. Adapted from Carrasco-Núñez et al. (2007).

Please cite this article as: Austin-Erickson, A., et al., Rhyolitic phreatomagmatism explored: Tepexitl tuff ring (Eastern Mexican Volcanic Belt), J. Volcanol. Geotherm. Res. (2010), doi:10.1016/j.jvolgeores.2010.09.007

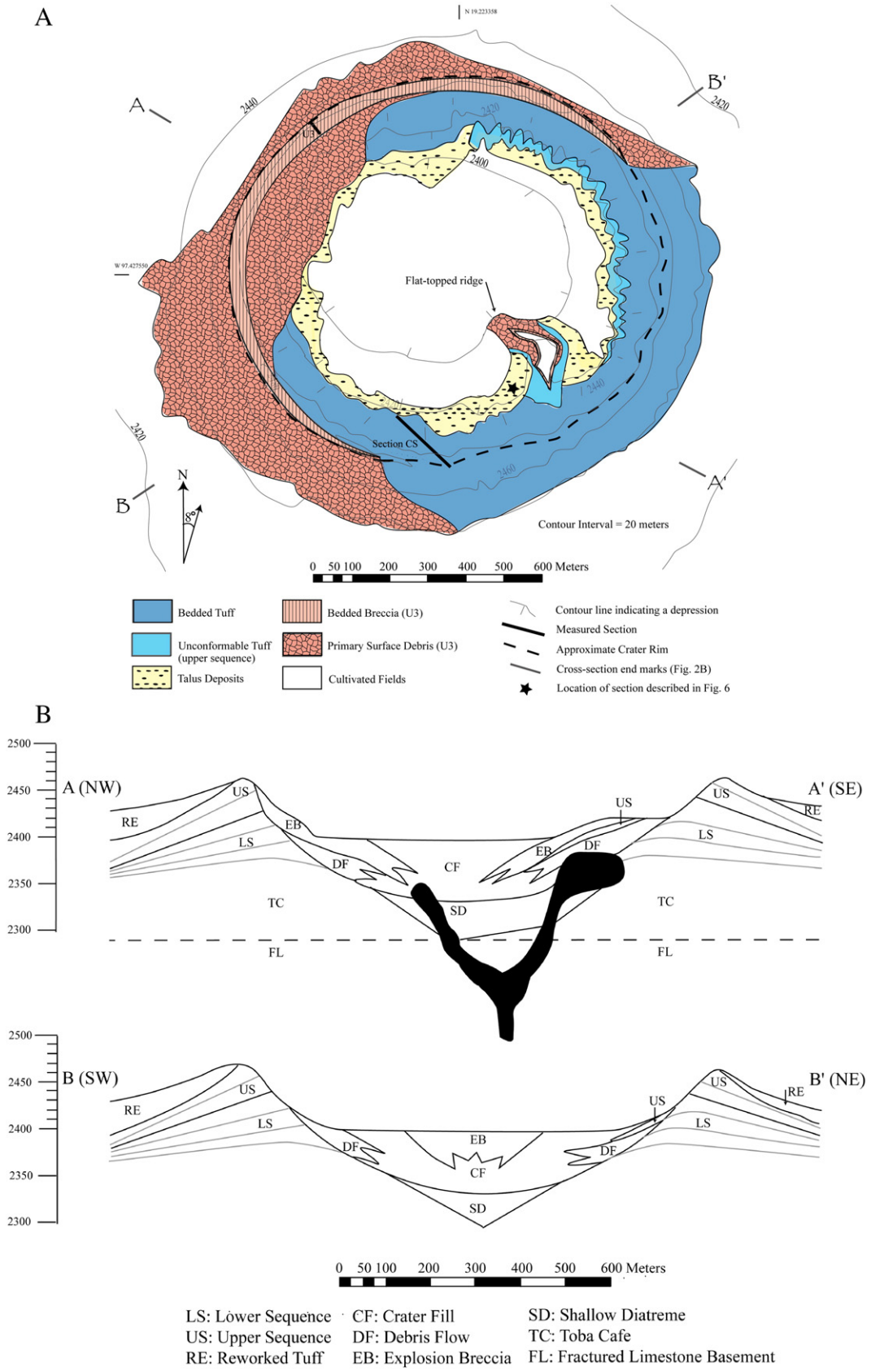

Fig. 2. (A) Surface morphology of Tepexitl. Section CS is a composite section, located along a roadcut. Bedded breccia is also referred to as U3 in the text (upper sequence unit 3) and was measured along the NW crater rim. The white areas both inside the crater and around the outer apron indicate active agricultural areas. (B) Schematic cross-sections through the crater are marked in (A).

Please cite this article as: Austin-Erickson, A., et al., Rhyolitic phreatomagmatism explored: Tepexitl tuff ring (Eastern Mexican Volcanic Belt), J. Volcanol. Geotherm. Res. (2010), doi:10.1016/j.jvolgeores.2010.09.007

material with time (Erickson, 2007; Austin-Erickson et al., 2008). From these results, a mechanism by which a highly viscous magma may react explosively with water is proposed. Because the fragmentation process is directly related to the amount of energy released by the system, these studies can be used in future research to determine the scale of eruption and the associated hazards specific to rhyolitic intrusions through saturated sediments, a realistic situation for future eruptions in active volcanic fields.

2. Field descriptions

Tepexitl crater has a diameter of approximately 1 km from rim to rim (Fig. 2A). The crater floor lies 20 m below the surrounding countryside and 75 m below the crater rim, but no contact was found with the pre-eruptive surface due to active agricultural cultivation on both the crater floor and the surrounding apron. The majority of crater-wall deposits are characterized by poorly cemented laminae to

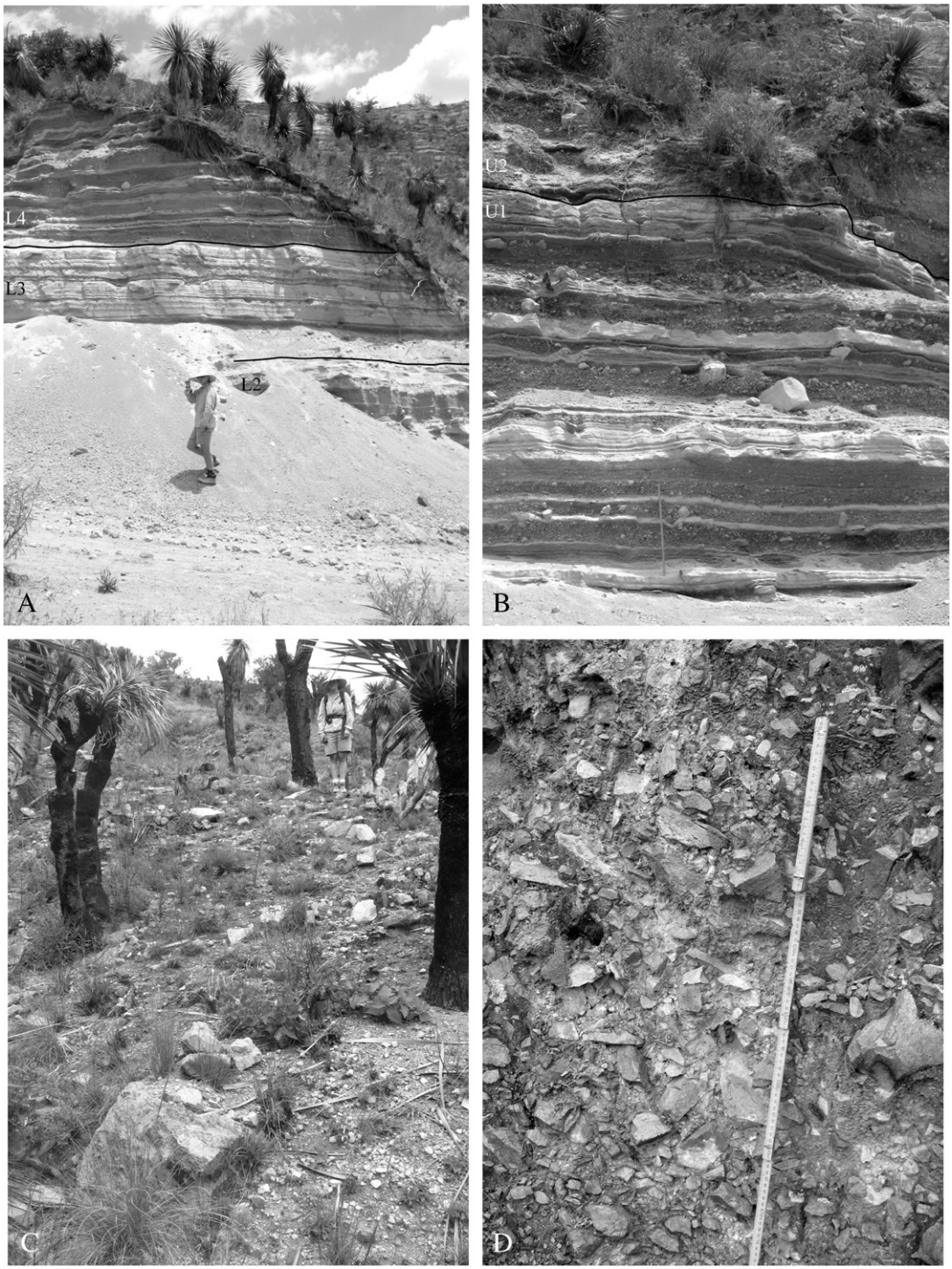

Fig. 3. (A) L2–L4 deposits as seen along the roadcut of Section CS, with person as scale and unit boundaries marked. (B) U1 and U2 deposits seen along Section CS, with 0.75-meter stick for scale and unit boundaries marked. (C) Angular blocks and other surface debris litter the slopes and drainages of the western crater. Person for scale. (D) Vertical outcrop of the surface debris deposit from a drainage mid-way up the western inner crater, with a 0.75 m stick for scale.

Please cite this article as: Austin-Erickson, A., et al., Rhyolitic phreatomagmatism explored: Tepexitl tuff ring (Eastern Mexican Volcanic Belt), J. Volcanol. Geotherm. Res. (2010), doi:10.1016/j.jvolgeores.2010.09.007

medium beds of fine-ash to coarse-ash tuff, with sharp contacts between beds.

The remarkably circular crater disguises a more complicated history, however, as the eastern and western sides of Tepexitl are distinctly different in surficial appearance. The eastern crater-walls are moderately well indurated with steep slopes composed of very well-exposed, thinly bedded tuff deposits that can be individually traced around the eastern crater rim and are easily accessible through steep drainages (Fig. 3A and B). The outer apron around the eastern half of the tuff ring also has steep drainages that expose primary sections of bedded tuff, which can be correlated to the inner crater units. The eastern half of the inner crater is also characterized by a 200-m-long, 15-m-high flat-topped ridge extending out from the SE crater wall (Fig. 2A and B).

In contrast, the slopes of western inner crater walls and outer apron deposits are not as steep, and are covered with vegetation and dominantly juvenile float debris, a combination that largely obscures any bedded tuff beneath it (Figs. 2 and 3C). The only visible bedded deposits occur as lapilli breccia in the uppermost 5 m near the inner crater rim (upper sequence unit U3, Fig. 2A), but cannot be correlated to beds in the eastern half of the crater. Additionally, large concentrations of fragmented breccia bombs and other distinct block textures are found in drainages around the western inner crater. Notably, the flat-topped ridge is also covered in similar debris and blocks.

Reworked talus material composed of massive to very-crudely-bedded, polylithic, very-poorly-sorted, matrix-supported deposits are found all along the inner crater floor. These wedge-shaped beds have a maximum thickness of 20 m, thinning in the direction of the crater center and commonly obscuring the base of early crater-wall deposits (Fig. 2). In the eastern half of the crater, the talus deposits are unconformably overlain by primary, steep inward-dipping beds (20°–30°) of layered tuff that contain intermittent laminae of accretionary lapilli and are plastically deformed by juvenile blocks.

Juvenile material throughout the Tepexitl deposits is peraluminous rhyolite (74–75% SiO_2) (Table 1), suggestive of origination from the same magma chamber. Juvenile material is poorly phyric (3–7 vol. % phenocrysts), with crystals that vary in size from 0.05 to 0.4 mm. Phenocrysts are dominated by quartz (35–40 vol.%) and plagioclase (30–40 vol.%), with sparse biotite and sanidine (each 10–20 vol.%) and accessory almandine. Juvenile textures are variably dense and devitrified with low vesicularity (herein called 'stony rhyolite', 20–25 vol.% vesicles), vitrophyric ('obsidian'), perlitic, brecciated, and flow-banded (Fig. 4), with few pumiceous textures observed in outcrop. Lithic clasts occur in different proportions throughout Tepexitl's deposits, and are consistent with Toba Café material (Erickson, 2007). The lithic clast compositions are predominantly recycled local volcanic clasts: andesite, basalt, altered rhyolite, and pumice, with a minor proportion of limestone clasts. Xenocrysts were only present in grain sizes 2-phi and smaller and include rounded sanidine, quartz, tourmaline, hornblende, and pyroxene.

Table 1
Normalized major-element XRF data for Tepexitl deposits.

Sample	SiO_2	TiO_2	Al_2O_3	F_2O_3t	MnO	MgO	CaO	Na_2O	K_2O	P_2O_5
	%	%	%	%	%	%	%	%	%	%
L2 (SR)	74.90	0.03	13.96	1.24	0.04	0.26	0.76	4.40	4.34	0.06
L2 (O)	75.02	0.03	14.04	1.15	0.04	0.19	0.74	4.52	4.24	0.06
U1 (SR)	75.11	0.03	14.02	1.21	0.05	0.17	0.71	4.33	4.32	0.05
U1 (O)	75.28	0.03	13.86	1.24	0.04	0.21	0.74	4.34	4.20	0.06
U3 (SR)	74.96	0.03	14.03	1.25	0.04	0.19	0.74	4.45	4.24	0.06
U3 (O)	74.94	0.03	14.02	1.24	0.04	0.20	0.75	4.47	4.26	0.06
Float (O)	75.08	0.03	13.83	1.30	0.04	0.17	0.73	4.45	4.30	0.06
Float (P)	74.87	0.03	14.04	1.34	0.04	0.15	0.75	4.46	4.26	0.06
Float (P)	74.99	0.03	14.04	1.15	0.04	0.19	0.74	4.52	4.24	0.06

Samples marked by stratigraphic unit and rock type, (SR = stony rhyolite, O = obsidian).

2.1. Western crater surface deposits

The 'surface debris deposit' on the western slopes of the tuff ring is up to several meters thick (as seen in drainages, thickening downslope), massive, clast-supported with an ashy matrix, monolithologic, and has an average clast size of 10 cm, with a range of 3–80 cm (Fig. 3D). The deposit is dominated by juvenile material, with breadcrust textures and jig-saw fracturing common. In isolated outcrops within drainages of the western inner crater, the deposit is pink in color, a feature that affects both large and small clasts alike (Fig. 5J). Exposed outcrops of underlying thinly bedded, fine-ash to fine-lapilli tuff deposits are rare, but do occur in eroded drainages. It is interpreted that this is a primary deposit that represents final activity of the eruptive sequence.

The uppermost feature of the western crater surface deposits are large juvenile blocks that litter the slopes and drainages and have textures not observed anywhere else within the stratigraphic sequence, including friable, breadcrust pumice clasts, fractured blocks of cemented juvenile-lithic matrix-supported breccias ('peperite bombs'), and fragmented perlite blocks (Fig. 5A–H). The dominant float blocks are angular stony rhyolite up to 2 m across.

The peperite bombs consist of angular, cemented chunks of matrix-supported, polylithic breccias that contain clasts of dominantly angular to rounded juvenile clasts and minor lithic clasts (Toba Café material, Erickson, 2007). Some clasts appear to be imbricated within the matrix and some have glassy rinds. The ashy matrix ranges from yellow to pink to gray. Rare lithic clasts are found as float. Another distinct texture found in the western crater is a veneer of yellow-altered clasts present only on the crater rim (the final deposit of U3; Fig. 5K).

2.2. The flat-topped ridge

A nearly complete cross-section of the flat-topped ridge's interior can be seen from its western drainage at the connection point with the inner crater (Fig. 6, map location in Fig. 2A). The basal >10 m consists of a massive, matrix-supported, very-poorly-sorted, polylithic deposit with clasts ranging from 1 mm to 20 cm in size. This is overlain by 1.5 m of laminated to thinly bedded tuff, with alternating fine-ash and coarse-ash deposits with sparse pods to discontinuous thin beds of accretionary lapilli. Rare bombs cause 5–15-cm-deep sags in the deposits. Overlying this tuff is approximately 1 m of massive, moderately-sorted, clast-supported, fines-poor, monolithologic breccia with angular juvenile clasts from 1 mm to 70 cm in size (dominated by stony rhyolite) — the same as the 'surface debris deposit' that overlies tuff deposits on the western inner crater. This same deposit is also found around the tip of the flat-topped ridge, with an average clast size of 7 cm and isolated patches of pink–red alteration that extend uniformly through the matrix and clasts. Another similarity to the western crater slopes is the high concentration of peperite bombs and friable pumice clasts around the flat-topped ridge. Some clasts found around the ridge have yellow alteration textures, similar to that found along the top of the western crater rim.

2.3. Stratigraphy

Crater-wall deposits, where observable, can be grouped into six unique facies, which change every 10 to 100 cm vertically and include three fine-ash tuff facies (Tl, AC, and Tlap) and three coarse-ash to fine-lapilli facies (Bt, Bl, and B; Fig. 7). These facies are present throughout the stratigraphic sequence, with sharp contacts between each deposit, a pattern suggestive of deposition by alternating surges and falls from discrete blasts. Changes in dominant facies and facies patterns define distinct units, which are used to analyze changes in eruptive dynamics with time.

Please cite this article as: Austin-Erickson, A., et al., Rhyolitic phreatomagmatism explored: Tepexitl tuff ring (Eastern Mexican Volcanic Belt), J. Volcanol. Geotherm. Res. (2010), doi:10.1016/j.jvolgeores.2010.09.007

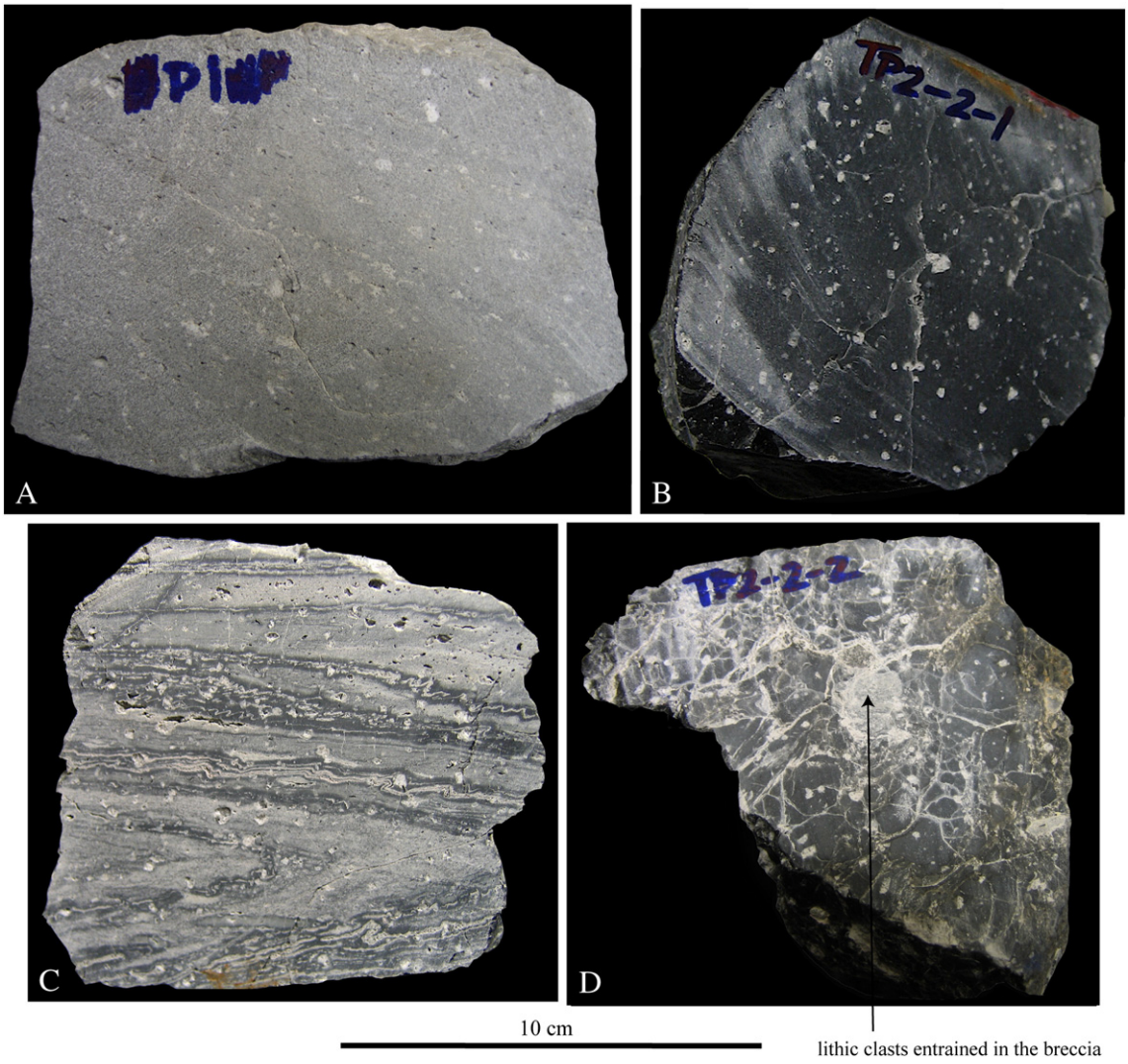

Fig. 4. Examples of typical juvenile block textures found in and around tuff ring walls. (A) stony rhyolite; (B) obsidian; (C) flow-banded; and (D) fractured obsidian with disseminated lithic clasts (dominantly basalt and andesite).

Two depositional sequences (upper and lower; Fig. 8) are defined by abrupt changes in clast size, dominant facies, block abundance and composition, and apparent water in the system (Table 2). The lower depositional sequence (5 units; L1–L5) is characterized by fine-grained, accretionary lapilli- and bomb-sag-rich, block-poor deposits, whereas the upper sequence (3 units; U1–U3) is distinguished by coarser-grained, block-rich deposits with no bomb sags (units are described in detail in Table 3). No bedded upper sequence deposits are found beyond the crater rim. Uncomformable tuff deposits in the eastern crater and deposits found on and around the flat-topped ridge are also associated with the upper sequence. The upper sequence is thicker in the western half of the crater, along the slopes where the surficial debris is present.

A composite section (CS) was measured along a 50-m roadcut in the southern inner crater and is the primary stratigraphic section used in analyzing changes in eruption conditions, due to the excellent exposure and accessibility of its deposits, with an average of 2 samples taken per meter (Fig. 9). Note the evolution of fine-grained early deposits to increasingly drier and coarser-grained deposits up-section, ending with the very coarse-grained deposits of U3 (measured along the NW crater rim; Fig. 8). The surface debris deposits of the western crater and flat-topped ridge described above are also considered part of U3.

3. Methods and results

3.1. Componentry

Samples were dry-sieved from −5 to 4.5 phi in half-phi intervals. A Coulter LS was used for analysis of grain size distributions from 4.5 phi to 11.5 phi. The SFT program (http://geodynamics.lanl.gov/Wohletz/SFT.htm; Wohletz et al., 1989) was used to analyze

Fig. 5. (A–H) Cut surfaces and hand samples of unusual block textures found as float blocks around the western inner crater and flat-topped ridge (with a 10-cm scale), including: A–C) friable breadcrust pumice with variable amounts of vesiculation, some with surface alteration; D–E) perlitic textures, both massive and flow-banded; and F–H) fragmented breccia blocks, variably monolithologic and polylithologic with gray, yellow, and pink ashy matrices, peperitic textures, and preservation of unusual pre-fragmentation contacts. I) Large block of stony rhyolite cemented to fragmented breccia, found in a western crater drainage. J) Pink alteration found in isolated deposits around western inner crater and the tip of the flat-topped ridge that pervades both clasts and matrix. K) The western crater rim has a thin veneer of yellow surficially altered rhyolite clasts (associated with deposit 5 of U3). These textures are all described in detail in Erickson (2007). (For interpretation of the references to color in this figure legend, the reader is referred to the web version of this article.)

Please cite this article as: Austin-Erickson, A., et al., Rhyolitic phreatomagmatism explored: Tepexitl tuff ring (Eastern Mexican Volcanic Belt), J. Volcanol. Geotherm. Res. (2010), doi:10.1016/j.jvolgeores.2010.09.007

Please cite this article as: Austin-Erickson, A., et al., Rhyolitic phreatomagmatism explored: Tepexitl tuff ring (Eastern Mexican Volcanic Belt), J. Volcanol. Geotherm. Res. (2010), doi:10.1016/j.jvolgeores.2010.09.007

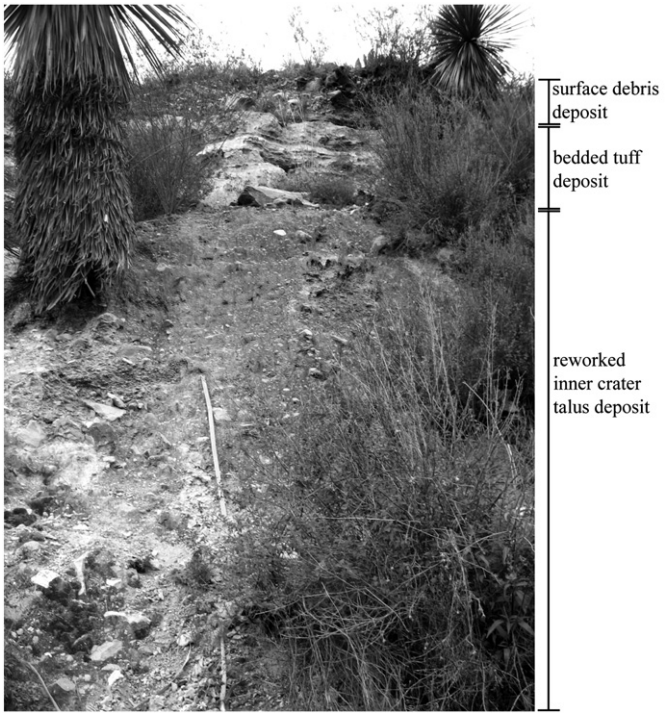

Fig. 6. Looking east up the flat-topped ridge from the southern-most drainage, with the same surface debris deposit capping the ridge as seen on the western crater slopes. 0.75-meter stick for scale.

subpopulations within these grain size data. The −2-, 0-, and 2-phi sizes were selected for componentry analysis based on the presence of repeated peaks in the grain size distribution around each of these modes. Based on these results, samples were chosen for LOI (Loss-On-Ignition) measurements, SEM analysis and experiment comparisons. Because the 2-phi grain size was determined to be the most significant with respect to fragmentation processes (Zimanowski et al., 2003; Erickson, 2007; Austin-Erickson et al., 2008), examination of component changes with time is limited to that range in this paper.

The three primary component categories identified in all samples are stony rhyolite, obsidian, and lithic clasts (Fig. 9). Armored lapilli are present in high concentrations in many lower sequence deposits. Dense to finely vesicular stony rhyolite clasts are the most abundant clast type within the majority of Tepexitl deposits, and generally increase up-section. Obsidian clasts are ubiquitous in all samples, concentrated in the coarse-ash and fine-lapilli grain sizes, and decrease in abundance with decreasing size (from 20 to 25 wt.% in the 0-phi size to less than 10 wt.% in the 2-phi size). The obsidian percentage in the 2-phi range does not change significantly with stratigraphic height in Section CS, but is present in higher concentrations in deposits from both the beginning and the end of the eruption. The ash-sized lithic components are consistent with Toba Café material (Erickson, 2007). Such lithic components can be the most important componentry variable, as they can record changes in eruption depth, both as downward penetration into underlying units (e.g. Houghton and Smith, 1993; Carrasco-Núñez et al., 2007), and as shallowing of eruptive center with time. Lithic grains are most abundant in the 2-phi size, and in the L1–L3 deposits, where they dominate in a few beds. Lithic percentages are variable but generally

	Facies	Description	Interpretation
fine-grained	Tl	Weakly laminated ash tuff with planar to mildly undulatory bedding and rare duneforms (1-3 cm in height). Scouring and bomb sags common along upper contacts with coarse-grained deposits in the lower sequence.	In the lower sequence, scouring, bomb sags, and weak smeary laminae are indicative of saltation and suspension processes operating in a low-particle-density wet surge (Fisher and Schmincke, 1984; Chough and Sohn, 1990; Sohn and Chough, 1992). Tl deposits in the upper sequence are the result of drier surges.
	AC	Mm-scale accretionary lapilli that fine outward and appear as: 1. discontinuous laminae to pods within fine-grained deposits. These accretionary lapilli are separated by a fine ash matrix. 2. Massive, thin- to medium-bedded deposits of accretionary lapilli-supported tuff.	1. Accumulation of ash into balls occurs because of cohesive forces in the shear layer of wet, low-temperature surges (Fisher and Schmincke, 1984; Dellino et al., 1990; Wilson and Houghton, 2000). 2. Hydrostatic attraction and consequent clumping of fine ash in a moisture-rich eruption environment, resulting in fall deposits (Sheridan and Barberi, 1983; Fisher and Schmincke, 1984).
	Tlap	Sub-cm-scale non-continuous laminae of alternating fine-ash tuff, coarse-ash tuff, and accretionary lapilli with occasional lapilli trains. Sharp internal, upper and lower contacts. Planar to undulatory bedding with rare dune forms (1-3 cm in height). Beds commonly deformed by bomb and lapilli sags in the lower sequence.	Traction and saltation deposits from density-stratified, rapid surge pulses (Sohn and Chough, 1992; Sohn and Chough, 1993; Branney and Kokellar, 2002). Lapilli trains can be caused by traction-carpet deposition (Fisher and Schmincke, 1984; Dellino et al., 2004) or by fall deposits that get 'caught up' in surges (Wilson and Hildreth, 1998).
coarse-grained	Bt	Massive, matrix-supported, very poorly sorted tuff-lapilli breccia. Intermittent, discontinuous weak laminae to pods of coarser ash and small lapilli. Most grains are coated in fine ash.	Column-collapse site with explosion maelstrom deposited close to the vent prior to any density stratification of clasts (Wohletz and Heiken, 1992) and/or a combination of early surge and fallout material causing unsteady flows and rapid deposition (Dellino et al., 2004). Ash coating suggests water-rich expulsion environment, which may have contributed to the unsteady surge pulses.
	Bl	Poorly sorted, massive, coarse ash to small lapilli breccia, mostly clast-supported but with weak, intermittent laminae of fine-ash tuff. Grading, both normal and reverse, is common. Commonly scours underlying fine-grained deposits. Occasional coarse grains are coated in fine ash.	Traction-carpet deposition of high-particle density surges (Dellino et al., 2001; Vazquez and Ort, 2006) and/or fall deposits, which can result in both normal and reverse grading (Houghton et al., 2000; Wohletz, 2001) and/or a combination of both, as suggested by the intercalation of intermittent laminae in coarse-grained material (Wilson and Hildreth, 1988).
	B	Massive, fines-poor, clast-supported lapilli breccia with moderately poor sorting. Mostly angular clasts. Graded in places, both normally and reverse.	Traction-carpet deposition of high-particle density surges (Dellino et al., 2001; Vazquez and Ort, 2006) and/or fall deposits from poorly energetic eruptive events (Sohn and Chough, 1992).

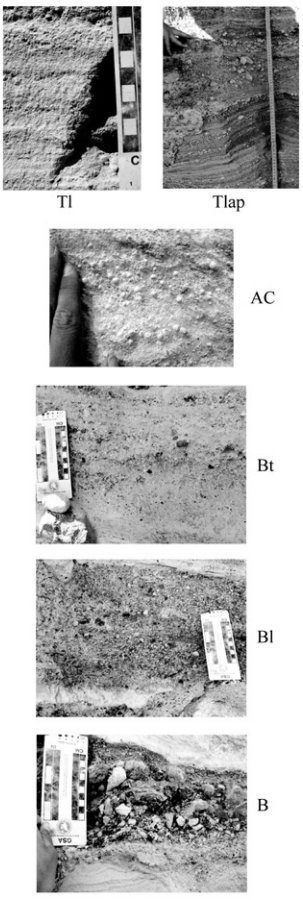

Fig. 7. Descriptions, interpretations, and photo examples of each facies type. (Interpretations from Sheridan & Barberi, 1983; Fisher & Schmincke, 1984; Wilson & Hildreth, 1988; Chough & Sohn, 1990; Dellino et al., 1990, 2001, 2004; Sohn & Chough, 1992, 1993; Wohletz and Heiken, 1992; Wilson & Houghton, 2000; Houghton et al., 2000; Wohletz, 2001; Branney & Kokelaar, 2002; Vazquez & Ort, 2006.)

Please cite this article as: Austin-Erickson, A., et al., Rhyolitic phreatomagmatism explored: Tepexitl tuff ring (Eastern Mexican Volcanic Belt), J. Volcanol. Geotherm. Res. (2010), doi:10.1016/j.jvolgeores.2010.09.007

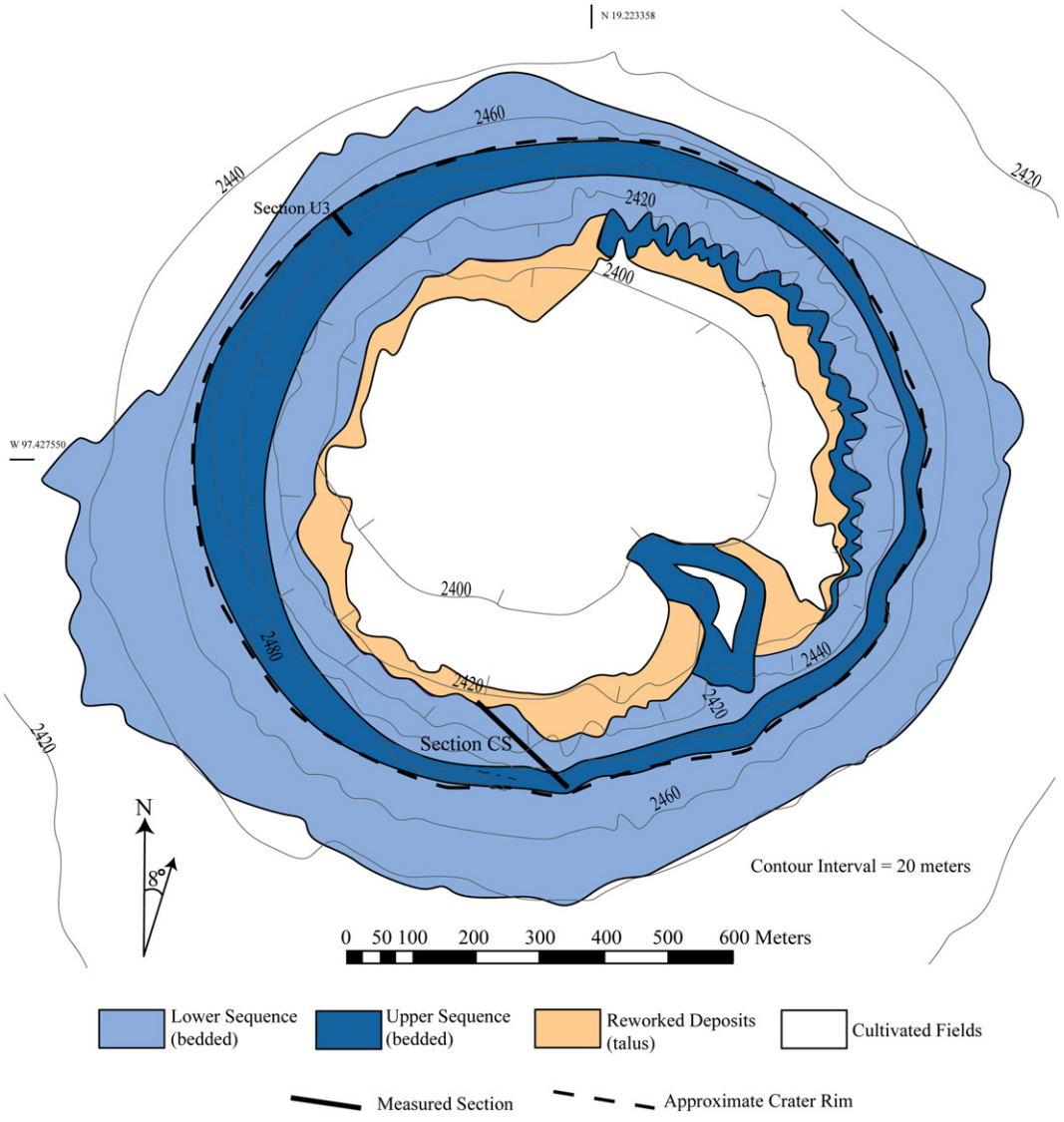

Fig. 8. Geologic map of Tepexitl tuff ring. Measured section locations are marked.

decrease through the eruptive sequence after deposition of unit L3. Armored lapilli are opaque, tan-yellow, dense round balls defined by a surficial "cement" that largely obscures the grain underneath and is composed of clear to yellow, very fine vitric ash. Partial removal of the cement on select grains reveals juvenile, lithic, and crystal cores.

3.1.1. Lower sequence componentry trends

Units L1–L3 are defined by abrupt facies and componentry changes, with spikes in lithic concentration that correspond to fine-grained beds. Lithic concentrations increase from a maximum of 37 wt.% at the base of unit L1 to a maximum of 54 wt.% at the top of unit L3. These units also contain the most abundant armored lapilli within the Tepexitl stratigraphy. In unit L1, obsidian has a peak of 24 wt.% at meter 4, the only place in Section CS where it occurs above its typical levels of between 3 wt.% and 15 wt.%. Armored lapilli concentrations peak in both the basal and top deposits of unit L2, at 29 wt.% and 33 wt.%, respectively.

In unit L4, lithic concentrations decrease from unit L3, varying between 11 and 32 wt.%. Armored lapilli are found only in fine-grained deposits in the middle of unit L4 at lower concentrations between 6 and 14 wt.%. Lithic concentrations in unit L5 progressively decrease to 15 wt.% at the top of the unit. Armored lapilli are present in fine-grained deposits in the middle of unit L5 at abundances of 6 to 8 wt.%, which corresponds to a peak in lithic clasts to 27 wt.%.

A repeating pattern of three distinct deposits, observed in the field exclusively in the lower sequence, has distinct componentry trends (Fig. 10, stratigraphic occurrences shown in Fig. 9). Each series of three deposits begins with: A) an obsidian-rich, coarse-grained breccia, with abundant iron-altered lithic clasts, sharply overlain by B) a highly deformed, fine-grained tuff deposit, rich in pumice, lithic clasts, and armored lapilli, sharply overlain by C) a coarse-ash tuff dominated by stony rhyolite, which, in some cases, contains armored lapilli. Each occurrence of this three-part series is composed of thinly bedded deposits and is characterized by rapid changes in componentry, grain size, and texture. This three-part depositional series

Table 2
Distinguishing field characteristics of lower and upper sequences.

Lower sequence	Upper sequence
Dominantly fine-grained facies	Dominantly coarse-grained facies
Abundance of deformed tuff	Less to no deformed tuff
Low abundance of blocks	High abundance of blocks
Blocks dominated by obsidian and lithic cobbles	Blocks dominated by stony rhyolite
Apron and distal deposits visible	No apron or distal deposits

Please cite this article as: Austin-Erickson, A., et al., Rhyolitic phreatomagmatism explored: Tepexitl tuff ring (Eastern Mexican Volcanic Belt), J. Volcanol. Geotherm. Res. (2010), doi:10.1016/j.jvolgeores.2010.09.007

Table 3
Unit Descriptions (depicted in Fig. 7) and Interpretations.

Unit	Description	Interpretation
Lower sequence		
L1	Deposits consist predominantly of medium-bedded facies Tl with 20–40 cm interbedded deposits of facies Bl. Fine-grained deposits are planar to wispy and discontinuous, mostly non-deformed thin beds to laminae. Scour channels and bomb sags increase up-section. Coarse-grained beds are laterally continuous with coarse grading (both normal and reverse). Scattered iron-altered clasts are present.	The fine-grained deposits likely result from highly efficient eruptions and resulting, increasingly wetter surges. In-situ iron-alteration of clasts to matrix is consistent with heat and water present during deposition. Field evidence is consistent with early-stage phreatomagmatic activity.
L2	Thinly bedded, alternating layers of facies Tl and Bl/Bt have sharp upper and lower contacts. Fine-grained layers are undulatory, discontinuous laminae with abundant bomb sags and scour channels. Coarse beds are continuous, fines-poor, and commonly crudely graded (both normal and reverse), with angular clasts that are commonly coated in fine adhering ash. Coarse beds commonly contain iron-altered lithic clasts.	The features seen in L2 are consistent with an increase in water:magma from L1, with continued heat present in the deposition system. It is interpreted that L2 resulted from high-energy, wet blasts and surges, conditions consistent with phreatomagmatism.
L3	L3 comprises a basal, thickly bedded, iron-clast- and obsidian-rich breccia (Bl) followed by a thick sequence of dominantly fine-grained tuff of facies Tl. The breccia is laterally continuous. The tuff is planar to undulatory with intermittent coarse-ash laminae and is characterized by occasional scour channels and lapilli sags.	The increase in fine-grained material, with similar textural features as lower units, points toward a period of increased eruptive efficiency of water-rich phreatomagmatic eruptions.
L4	Deposits are dominated by thinly- to thickly bedded Bl facies, with thinly interbedded, planar to undulatory tuff beds that contain sparse bomb sags and scour channels. Breccia layers contain rare iron-altered clasts and are continuous, fines-poor, and commonly graded — both normal and reverse. L4 is the coarsest-grained and most voluminous sequence of the entire tuff ring, but it thins rapidly from the inner crater toward the apron (as seen from a roadcut along composite Section CS — location on Fig. 2A).	The coarse-grained nature, large volume of erupted material, large percentage of blocks, and rapid lateral thinning are evidence that L4 likely resulted from lower efficiency eruptions than deposits lower stratigraphically (both fragmentation and depositional systems), with most deposition occurring near the vent. However, deformed tuff indicates water was still present in the eruptive system and occasional iron-clasts indicate some degree of heat was present during deposition. L4 was also a time of crater widening (Erickson, 2007).
L5	Planar to slightly-undulatory Tl and Tlap facies dominate, with interbedded deposits of AC facies. Minor, thinly bedded, reversely-graded, obsidian-rich, coarse-ash to small-lapilli deposits of Bl facies have fine-ash-coated grains and iron-altered clasts. Fine-grained tuff contains abundant scour channels and bomb/lapilli sags.	Textures consistent with heat and water in the eruptive system. Dominantly fine-grained deposits were likely deposited by high-energy, wet surges and blasts that may have resulted from phreatomagmatic eruptions.
Upper sequence		
U1	Thin- to medium-bedded, coarse-grained deposits of Bl facies dominate, with interbedded laminae to thin layers of tuff decreasing up-section. Coarse-grained breccias are laterally continuous with both normal and reverse crude grading. Intermittent fine-ash tuff is planar to undulatory with rare bomb sags and scour channels in the lowermost deposits.	Bomb sags and scour channels low in the unit are consistent with some water in the eruptive system, but a progressive decrease in water:magma occurs during deposition of U1. The coarse-grained deposits of U1 are interpreted to have formed from low-energy and/or low-efficiency eruptions.
U2	At the base of U2, deposits of Bt facies dominate and are ash-rich, continuous, and planar with crude grading (both normal and reverse). Facies Tlap/Tl and B/Bl are interbedded toward the top, with fine-grained, laminated deposits more abundant than in underlying U1. The fine-grained deposits are planar and non-deformed with no scour channels or bomb sags.	The decrease in ash deformation (no scour channels or bomb sags) suggests that U2 was the result of dry surges from a lower water:magma ratio in the vent area. The abundance of fine-ash may relate to phreatic eruptions through crater fill or to primary fragmentation processes.
U3	U3 is a 5-m section measured at the top of the western crater rim and is distinct from all previously described units. It is dominated by thickly bedded, coarse-grained, clast-supported, fines-poor deposits of facies B, with angular, juvenile clasts and very-thinly-interbedded tuff deposits. Breccia composition changes laterally, with obsidian and flow-banded material present in high concentrations at the top and bottom of the unit. The middle of the unit is dominated by stony rhyolite blocks that have occasional breadcrust textures. The uppermost deposit is a thin bed of pumice- and obsidian-rich, yellow-coated lapilli and coarse-ash clasts. This deposit also contains coarse-ash-sized fragmented juvenile breccia clasts.	The thick, coarse-grained, texturally- and compositionally- diverse, angular deposits of U3 contain no visible lithic clasts and are most consistent with dome/plug explosion at the end of the Tepexitl-forming eruption. The yellow coating on the final deposits may result from secondary alteration or vent-related alteration.

occurs repeatedly and appears to represent an important eruptive process during the deposition of the lower sequence.

3.1.2. Upper sequence componentry trends

Upper sequence units U1–U3 componentry patterns are defined by overall decreased lithic concentrations and distinct end-of-eruption trends (unit U3). Lithic concentrations in unit U1 decrease progressively from 12 wt.% at the base of the unit to 0 wt.% at the top of the unit. A spike of both armored lapilli (15 wt.%) and lithic grains (34 wt.%) at meter 34.3 corresponds to a thinly bedded B-facies deposit, and is the only occurrence of armored lapilli in the upper sequence. In unit U2, lithic concentrations vary between 5 and 17 wt.%, but these grains appear more rounded and weathered than lithic grains from stratigraphically lower deposits (Erickson, 2007). Obsidian concentrations are 21 wt.% at the top of unit U2, and progressively increase throughout unit U3 deposits.

Bedded U3 deposits are only observed as a 5-m-thick section on the top of the western crater rim, perhaps due to directed blasts in that direction. These are all fines-poor, clast-supported B-facies deposits (as described in Fig. 7) with distinct componentry patterns, angular clasts, and sharp contacts between beds. About 5–10 cm of tuff separates each B-facies deposit (as seen in Fig. 9). Lithic clasts are notably absent in all deposits. Stony rhyolite makes up the remainder of the juvenile percentages given in the following descriptions. Sampled beds (labeled in Fig. 9), from bottom to top, consist of: (1) a 40-cm pumice-rich (38 wt.%), obsidian-rich (25 wt.%) coarse-lapilli deposit; (2) a 50-cm-thick stony rhyolite-dominant, coarse-lapilli deposit with minor pumice (18 wt.%) and obsidian (10 wt.%) overlain by 15-cm of well indurated accretionary lapilli; (3) a 3-m thick deposit with coarse-lapilli to blocks of angular stony rhyolite (90 wt.%); (4) a 70-cm coarse-lapilli deposit with abundant obsidian (32 wt.%) and minor pumice (11 wt.%); and (5) a 15-cm fine-lapilli deposit dominated by yellow-altered armored clasts (60 wt.%; Fig. 4K). The origin of the yellow alteration is unknown, and is stratigraphically limited to this deposit. Obsidian is slightly less abundant than in sample 4, although it is still a significant

Please cite this article as: Austin-Erickson, A., et al., Rhyolitic phreatomagmatism explored: Tepexitl tuff ring (Eastern Mexican Volcanic Belt), J. Volcanol. Geotherm. Res. (2010), doi:10.1016/j.jvolgeores.2010.09.007

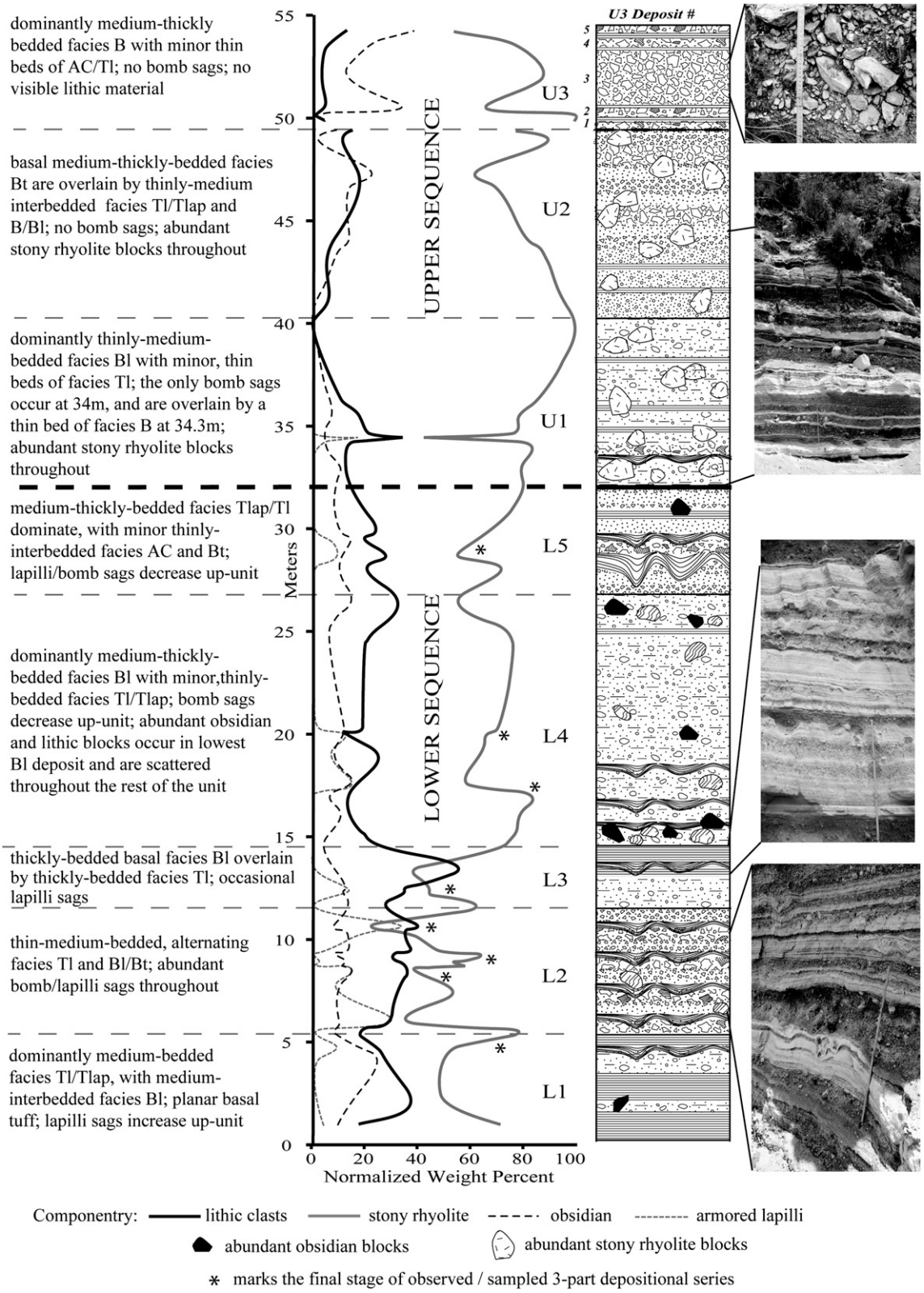

Fig. 9. Generalized stratigraphic section for Tepexitl crater-wall deposits is stylized to represent the patterns and deposits seen in the field, with normalized percentages of major component categories for 2-phi grains shown to the left. Componentry lines have been smoothed, and are the result of 48 data points. The thick black dashed line marks the boundary between the upper and lower sequences. Meters 0–50 represent Section CS. U3 was measured along the western crater rim (refer to Fig. 8 for locations of measured sections). U3 deposits are described in detail in the text. See detailed unit descriptions in Table 3. Scale in all pictures is 0.75 m.

component (23%). Nonaltered pumice and stony rhyolite are present in very small percentages (<10%), and there is a very slight increase in lithic grains in this deposit (6 wt.%). A small percentage of fragmented peperite clasts in the 2-phi size range appear to be smaller versions of the large peperite bombs found as western inner crater float blocks.

Please cite this article as: Austin-Erickson, A., et al., Rhyolitic phreatomagmatism explored: Tepexitl tuff ring (Eastern Mexican Volcanic Belt), J. Volcanol. Geotherm. Res. (2010), doi:10.1016/j.jvolgeores.2010.09.007

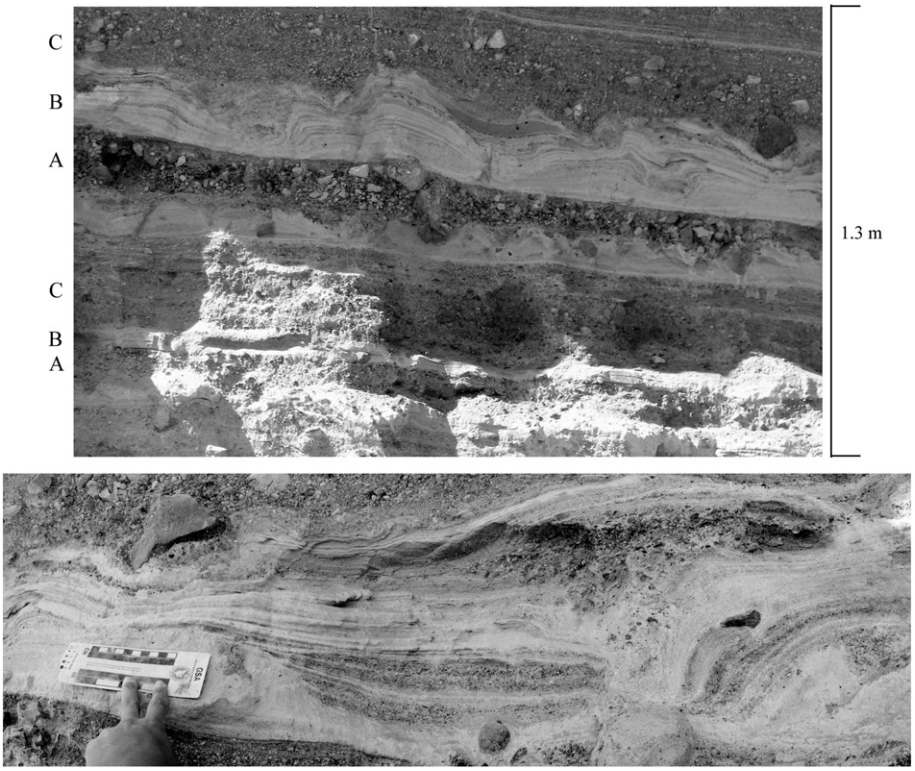

Fig. 10. Three-part depositional series photos. A) Two progressions of the three-part depositional series from Section CS, L2, meters 8.5 to 9.8. Note the thinly bedded nature of each individual deposit. B) Striking cohesive deformation of upper deposit is shown in the lower photo, a feature typical of this sequence.

3.2. Loss-On-Ignition volatile data

Loss-On-Ignition (LOI) is a measurement of the amount of water and other volatiles a sample loses at low (meteoric) and high (magmatic) temperatures. Lapilli of obsidian and stony rhyolite of a single representative sample from each unit (2-phi size, multi-grain samples, separated by microscope examination) were selected to collect LOI data at both 200 °C (post-emplacement hydration) and at 1000 °C (magmatic water vapor and some gases; Fig. 11). Additionally, one breadcrust pumice float block from the western crater was analyzed. All samples had significant magmatic water, which indicates that the system was incompletely degassed throughout the eruption.

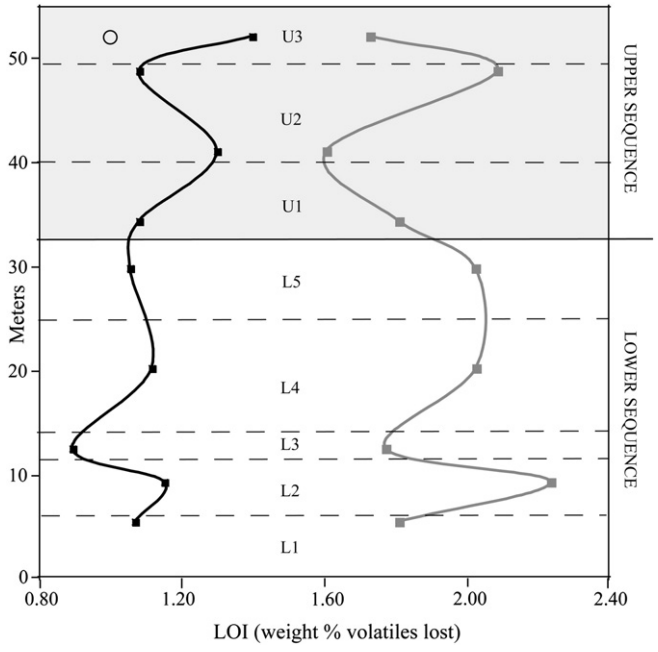

Fig. 11. Loss-On-Ignition values at 1000 °C for obsidian (black line on left) and stony rhyolite (gray line on right), plotted against stratigraphic height. The open circle in U3 is pumice collected as a float block from the western crater surface debris deposit.

Several patterns emerge: (1) LOI values for obsidian are consistently lower than those for the corresponding stony rhyolite in the same bed; (2) the lower sequence is characterized by an LOI variation pattern that is parallel for obsidian and stony rhyolite; and (3) the upper sequence is characterized by obsidian and stony rhyolite LOI patterns that mirror, rather than mimic, each other.

3.3. Petrography of sample 2-2

Petrography will only be discussed here with regard to Sample 2-2, a clast of obsidian breccia collected from meter 5.8 of Section CS in unit L2 (seen in Fig. 4, picture D). Cut surfaces reveal a highly complex fracture network and brecciation pattern, with visible, disseminated lithic clasts between 2 mm and 15 mm in diameter (Fig. 12). Thin-section examination exposes a distinct pattern. The network of fractures seen in hand sample are filled with fine-grained lithic grains and xenocrysts from sub-mm size to 3 mm in diameter. 75–80% of the fracture volume is composed of mostly rounded, poorly sorted lithic grains, consistent with Toba Café deposits (Erickson, 2007). These grains include basalt, palagonitic glass, limestone, crystalline rhyolite, andesite, and xenocrysts of olivine, hornblende, and muscovite. Individual lithic grains are enclosed in a glassy fine-grained matrix (the remaining 20–25% of the fracture volume), which has a higher concentration of equigranular groundmass microlites than the matrix of the obsidian 'host'. The fracture networks show no bedding structures or flow alignment. Fracture thickness varies from sub-mm to mm-scale. Fractures and associated lithic grains account for approximately 30% of the slide by volume.

Please cite this article as: Austin-Erickson, A., et al., Rhyolitic phreatomagmatism explored: Tepexitl tuff ring (Eastern Mexican Volcanic Belt), J. Volcanol. Geotherm. Res. (2010), doi:10.1016/j.jvolgeores.2010.09.007

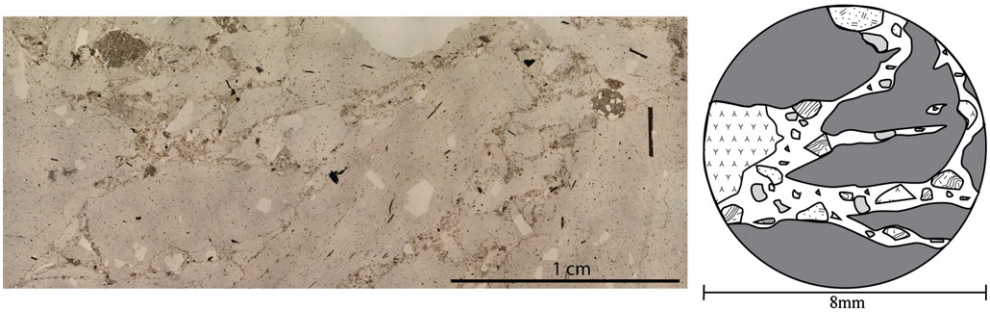

Fig. 12. A) Photomicrograph of an obsidian breccia sample taken from Section CS unit L2. The obsidian host is cut by a network of fractures, in which poorly sorted lithic grains and xenocrystals are concentrated in a matrix of lithic ash. B) A detailed sketch of this texture, with the dark gray area representing the obsidian host, the white area representing the ash matrix, and the grains indicative of individual lithic fragments.

4. Discussion

Morphologic, stratigraphic, and grain analyses point toward a change in eruptive regime between deposition of the lower and upper sequences. The deposits of the lower sequence indicate abundant external water was present in the eruptive system, which appears to be associated with a high efficiency of fragmentation (fine-grained deposits with few large blocks). Lithic fragments indicate that the source of water during the eruption was saturated sediment from a shallow, sandy aquifer (Toba Café). The upper sequence deposits, however, are consistent with drier eruptive conditions. These coarser-grained, thicker-bedded, and block-rich deposits are consistent with less efficient fragmentation processes. This eruptive pattern is broadly interpreted as resulting from high-energy phreatomagmatic eruptions (lower sequence) grading into lower-energy magmatic-dominated eruptions (upper sequence), which occurred as external water was reduced within the system and/or as the magma plug shallowed.

4.1. Interpretation of the lower sequence

Componentry analyses reveal patterns in stony rhyolite and lithic concentrations that are consistent with unit boundaries observed in the field, and appear to mirror changes in the fragmentation regime (Fig. 9). The evidence suggests that phreatomagmatism was most efficient during deposition of units L1–L3, in which lithic concentrations are highest. Sharp increases in lithic grains have been directly associated with an increase in the potential amount of external water available to the eruptive system (Houghton and Smith, 1993). Lithic material at Tepexitl is from a shallow, fine-grained aquifer, and could increase in a deposit either from shallow vertical migrations of low-energy phreatic explosions through overlying material, or from a downward-migrating explosion locus that penetrates into underlying lithic material. L1–L3 show a systematic increase of lithic concentration within the fine-grained beds, as well as a progressive increase in the degree of deformation of deposits, most consistent with an eruptive center progressively deepening into underlying Toba Café. The gradual decrease in lithic concentration from L4 through the upper sequence is consistent with explosions that penetrated through less and less overlying material, a condition met by an end to excavation concurrent with dome growth during this phase and shallower eruption centers.

The large average size of the obsidian clasts compared to stony rhyolite and the low weight percentage of obsidian clasts in all deposits regardless of eruptive regime indicate that obsidian was likely present at some distance from the locations where the most fragmentation energy was concentrated, also consistent with phreatomagmatic/magmatic processes of a slowly rising plug. The three-part depositional series (Fig. 10) observed in the lower sequence may be common in rhyolitic phreatomagmatism. A similar pattern of obsidian, pumice, and lithic-rich beds were observed in Fryiplaka tuff ring, a series that also grades into coarser-grained stony rhyolite with time (Campos Venuti and Rossi, 1996). At Tepexitl, the pattern is associated with features that indicate heat and water were present in the eruptive system, as well as compositional indicators for phreatomagmatic explosions.

4.2. Mechanism for phreatomagmatic fragmentation at Tepexitl

Patterns observed in Tepexitl deposits are evidence that coarse mixing of a high viscosity melt and external water can occur, but the manner and mechanism for such mixing needs to be explored. Zimanowski et al. (1997) emphasize that it is the rate of transfer of thermal energy to mechanical energy that governs phreatomagmatic efficiency, which in turn depends on the interfacial surface area available to coarsely mix. In low-viscosity magmas, this interfacial area is very uneven and so has a large surface area. An increase in viscosity decreases this topography and thus decreases the amount of surface area exposed to coolant, which would limit explosivity and intensity of eruption (Zimanowski et al., 1991). With a highly viscous rhyolite magma, interfacial melt instabilities (Rayleigh-Taylor and Kelvin-Helmholtz) are probably incapable of initiating phreatomagmatism.

As highly viscous magma exhibits both brittle and ductile behavior during ascent, with repeated fracture and re-annealing of the marginal obsidian (Tuffen et al., 2003; Rust et al., 2004; Gonnermann and Manga, 2005), it is proposed here that the requisite surface area needed for efficient heat exchange can be accomplished by hydraulically-driven intrusions of liquefied sediment into fractures that develop along the conduit walls/rising plug during emplacement (as evidenced in Sample 2-2; Fig. 12). Fluidization of an impure coolant (such as saturated sediment) can occur during emplacement of a magma body and is well documented as a key process in the formation of peperite, which results in a complex network of fractures in the igneous body being pervaded by sediment (e.g. Kokelaar, 1982; Heiken et al., 1988, Dadd and Van Wagoner, 2002). If the fragmented lava is more permeable than its surroundings, high pore pressures will drive the fluidized sediment into rapidly forming fractures, into the hotter interior of the melt and beyond the quenched exterior (Wohletz and Heiken, 1992; Dadd and Van Wagoner, 2002; Gutmann, 2002).

Vapor film collapse along these fractures would allow for direct contact of coolant and melt, initiating heat transfer in a confined environment — an experimentally determined requirement for MFCI (Morrissey et al., 2000). If energy released during this process was greater than the overlying lithostatic pressure, a phreatomagmatic explosion would ensue. It is likely that fine fragmentation would occur during initial contact of this process, despite the limited coarse mixing, generating active particles (grains produced directly on the magma:water interface whose surface area reflects the high

Please cite this article as: Austin-Erickson, A., et al., Rhyolitic phreatomagmatism explored: Tepexitl tuff ring (Eastern Mexican Volcanic Belt), J. Volcanol. Geotherm. Res. (2010), doi:10.1016/j.jvolgeores.2010.09.007

fragmentation energy generated during thermohydraulic coupling; Büttner et al., 2002.

Microscopic examination of Sample 2-2 provides evidence for such fluidization and mingling at Tepexitl. The high concentration of xenocrysts in the fractures of this breccia indicates that Toba Café sediment and juvenile material were interacting in the early stages of eruption during deposition of the lower sequence. However, the preservation of sediment intrusions into fractures (Sample 2-2) indicates that such explosive behavior does not happen along the interface of every fracture, and that the volume of fractures/interface area, as well as the degree of cooling of the melt likely plays a large role in the ability of heat transfer to be effective. The link between water intrusion into fractures and subsequent eruption has already been documented for dome explosions following heavy rainfall events (e.g. Mastin, 1994; Elsworth et al., 2004) and is a viable explanation for triggering these explosions as well. Experiments confirm that this is a viable mechanism for rhyolitic phreatomagmatic fragmentation: the only way found to trigger phreatomagmatic eruptions of rhyolitic melt made from Tepexitl stony rhyolite was to cover the surface of the plug with water and then bulge the melt upward, generating cracks into which water then penetrated (Austin-Erickson et al., 2008).

Waning phreatomagmatic activity with time could be caused by the formation of a cone of depression (Lorenz, 1986), which would decrease the amount of water in the eruptive system. It is also possible that insulated conduits, or lava tubes, are created by margin chilling and channel hot magma upward through the sandy aquifer, effectively 'sealing' off the hot interior from the saturated sediment coolant as the eruption progresses and evolves into a dominantly magmatic sequence. Such a process would account for the paucity of obsidian blocks in upper sequence deposits. Another variable to consider is that phreatomagmatic eruptions of a viscous magma may require a moderate 'injection' velocity of the magma into the coolant in order to promote MFCI, and this would dominantly occur during initial emplacement.

The three-part depositional series observed in the lower sequence may represent a rapid succession of eruptions occurring when external water intrudes into cracks in the exterior of the rising plug, causing a phreatomagmatic explosion. If the locus of explosion is inside the crack, obsidian around the crack would be ejected first, then phreatomagmatically-fragmented juvenile material and surrounding saturated lithic material ejected as a wet surge. The high concentration of pumiceous clasts in the second layer of this series relative to other Tepexitl deposits may be related to shock-wave-triggered fine vesiculation of melt adjacent to the water–magma interface, known to occur during rapid decompression (Dellino et al., 2001; Ichihara et al., 2002; Lorenz and Haneke, 2004). Armored lapilli in Tepexitl deposits are restricted to these water-rich, hot deposits. Rapid decompression of the system may also explain the final deposits — shock waves cause brittle failure and magmatic response, possibly ejected as a fall deposit.

Scanning electron microscope images of the particles in the lower and upper sequences reported by Austin-Erickson et al. (2008) also support a change in eruptive regime from phreatomagmatic to magmatic in the lower to upper sequences. Active particles (grains with distinct surface textures that form directly on the water:magma boundary; Büttner et al., 2002) are found exclusively in lower sequence deposits at Tepexitl, and are particularly associated with the three-part depositional series. Experiments demonstrate that these particles resulted from phreatomagmatic fragmentation (Erickson, 2007; Austin-Erickson et al., 2008). Upper sequence deposits contain only passive particles (no hydromagmatic surface textures; Büttner et al., 2002), consistent with magmatic fragmentation.

4.3. Interpretation of the upper sequence

The upper sequence deposits are coarser-grained, have no visible or sampled three-part depositional series, are restricted to the inner crater, and appear to be associated with drier eruptive conditions. The evidence points toward a likely shallowing of both the magma plug and the level of fragmentation, with a shift toward dominantly magmatic processes. The spike of lithic clasts and armored lapilli in unit U1 (Fig. 9) are interpreted to result from a 'vent-clearing' eruption that recycled earlier erupted material concurrent with the shallowing of the magma plug. The eruptive events that deposited the final beds of unit U1 incorporated no lithic material, which is most consistent with an eruptive center above the level of crater fill. The rounded, weathered-looking lithic clasts visible in U2 deposits are also consistent with low-energy phreatic eruptions that recycle crater fill. The final eruptive phase of Tepexitl caused deposition of U3, which includes both a bedded sequence of deposits limited to the western crater rim, as well as the juvenile blocks found on the surface of the western inner crater and the flat-topped ridge.

The lack of a dome within the crater implies either that the magma plug did not rise much above the level of crater fill, or that a small dome did emerge, but 'self-destructed', leaving no morphologic trace. Evidence to support both a shallowing of eruptive locus during deposition of the upper sequence and the existence of a small dome at the end of the eruption includes: (1) the dominant block composition changed from obsidian/lithic in the lower sequence to stony rhyolite in the upper sequence (ejection of dome/plug interior versus rapidly quenched exterior in a water-rich environment); (2) lithic clasts are notably absent from the upper sequence, particularly from U3 (Fig. 9); (3) distinctive juvenile textures (breadcrust pumice, fragmented breccia blocks and perlite) are found as large blocks only on the surface (not in earlier deposits) and are consistent with textures found in a dome (Manley and Fink, 1987); (4) the coarse-grained, matrix-poor, angular juvenile deposits of U3 with jig-saw fractures in blocks and lapilli indicates primary deposition (little to no reworking); and (5) the pink color of some U3 deposits indicate primary deposition with heat.

The sequence observed in the U3 deposits is also consistent with explosion of a small dome with internal textures as described in Manley and Fink (1987) and Fink and Manley (1987). The rapid changes in juvenile componentry suggest that the explosion center migrated progressively through the textural sequence from the dome top to the dome base. The deposits from top to bottom represent an "upside-down" dome, with the stratigraphically lowest samples representing the uppermost part of the dome (Fig. 13). The tuff layers between each breccia deposit in U3 indicate that explosion occurred by distinct blasts, which correspond to componentry changes.

Deposits 1 and 2 are the lowest stratigraphically and show a progressive decrease in pumice and obsidian, typical textures found when moving from the surface of a dome toward its interior. Deposit 3 is the thickest deposit, with the coarsest-grained clasts and the most stony rhyolite component, consistent with eruption of a dome interior. Deposit 4 is obsidian-rich, consistent with the basal obsidian observed in dome cross-sections. Deposit 5 is slightly unusual, in that it contains fragmented peperite breccias and hardened surficial yellow coatings on many of the clasts. One possible interpretation of these textures and components is that this small deposit represents a final explosion through the lowermost breccia of the dome and underlying hydrothermally altered and cemented material — indicators that the dome was completely destroyed (or nearly so), with any evidence of it covered by crater fill. Peperitic textures within these breccia clasts indicate that groundwater may also have been present in the crater area during the final eruptions, and may have played a role in the dome removal process. The distinctive textures of scattered blocks found as debris on the western slopes (Fig. 5) also support this interpretation: perlitic textures, breadcrust pumice, and fragmented polylithic peperitic breccia blocks with yellow to red matrices are all associated with dome textures.

The evidence suggests that external water likely played a role in the final dome explosion at Tepexitl, although the mechanism(s) for

Please cite this article as: Austin-Erickson, A., et al., Rhyolitic phreatomagmatism explored: Tepexitl tuff ring (Eastern Mexican Volcanic Belt), J. Volcanol. Geotherm. Res. (2010), doi:10.1016/j.jvolgeores.2010.09.007

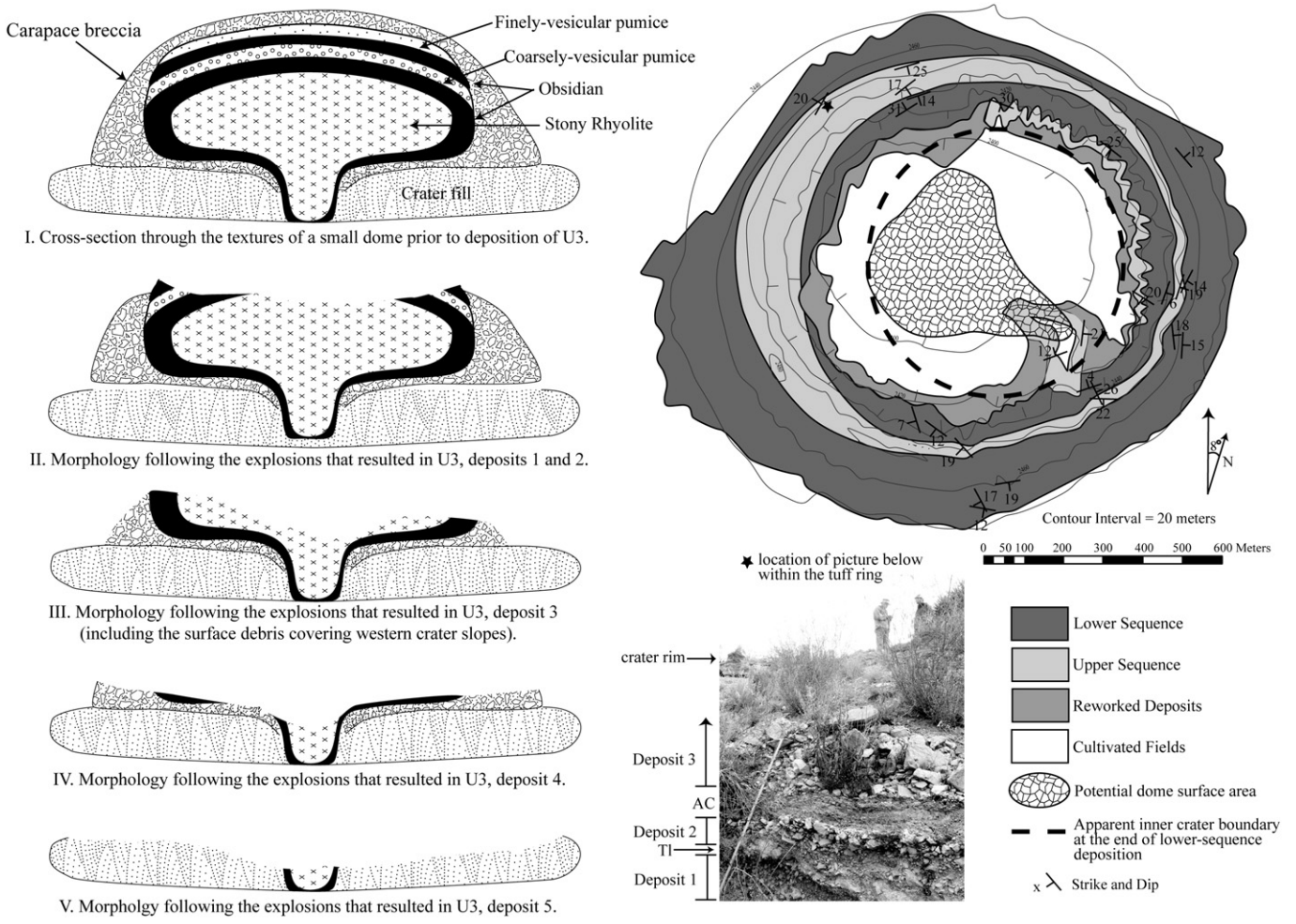

Fig. 13. A) An idealized model of step-by-step retrogressive dome explosions (I–V), based on componentry analyses of U3. Dome facies are based on Manley and Fink (1987). B) A potential dome configuration within the inner crater. The boundary between the upper and lower sequences is inferred to be the crater rim location when dome growth began. Strike and dip angles indicate that the final explosions widened the crater to the west (present shape), with the apparent lower sequence crater floor location shown by the dashed line. Due to extensive surface debris, no strike and dip measurements could be recorded in the western half of the crater. C) Field picture showing the U3 stratigraphy of Tepexitl. A 0.75-meter stick is for scale.

explosion is not fully understood, and probably involved some combination of magmatic, weather-related, and phreatomagmatic triggers. As the magma was only partially degassed upon extrusion, internal pressure build-up within the dome interior may have triggered explosion. It is also possible that rainwater seeping into surface cracks on the dome triggered phreatomagmatic explosions, as has been documented at domes elsewhere (Mastin, 1994; Elsworth et al., 2004), and may be the reason for the accretionary lapilli found in U3. Phreatomagmatic activity from groundwater may also have played a role in the explosion, as blocks of cemented crater fill and blocks coated with a yellow alteration or with peperitic textures occur in the final breccia, implying that water was present beneath the dome during intrusion and/or at the end of the eruption. The basal breccia of domes commonly have blocky peperitic textures from mixing with fluidized wet sediments or crater fill upon extrusion (Kokelaar, 1982; Bonnichsen and Kauffman, 1987; McPhie et al., 1993; Dadd and Van Wagoner, 2002) and these blocks may represent that process at Tepexitl. The 'peperite bombs' found around the surface of Tepexitl likely represent a combination of cemented crater fill, carapace breccia, and/or preserved peperitic interaction between rising magma and saturated crater fill. It is possible that cementation was caused by a shallow hydrothermal system associated with the rise of magma as a shallow intrusion. This final stage may have appeared as a dome growing in a 'tuff pond' of soupy crater fill. A similar process of retrogressive dome explosions is described by Adams et al. (2006) for a dacitic pyroclastic series deposited during the 1912 eruption of Novarupta. The final blocks associated with this eruption including flow-banded, pumiceous, and dense juvenile clasts, commonly with breadcrust textures, as well as fragmented breccia clasts presumed to be from the dome carapace (similar to those found at Tepexitl). Adams et al. (2006) conclude that dome explosion at Novarupta was due to a combination of incomplete degassing and external water, perhaps rainwater.

A dome configuration such as that in Fig. 13 would account for the presence of unconformable tuff deposits limited to the eastern inner crater, possibly having originated from marginal pyroclastic explosions of a dome growing through saturated crater fill during deposition of the upper sequence, ejecting low-energy surges that remained within the crater. Strike and dip angles indicate that the final explosions widened the crater to the west, which accounts for the greater apparent thickness of the upper sequence in the western half of the crater and the isolated presence of surface debris on the western inner slopes (Fig. 13). There is no evidence for significant repose periods during this process. Complete destruction of a dome during the eruption itself is likely unusual and may depend upon a small original volume of the dome. An estimate of the volume of material erupted during deposition of U3 is 2.3×10^6 m^3, or 15% of the total volume of the tuff ring (including U3 deposits as well as western

Please cite this article as: Austin-Erickson, A., et al., Rhyolitic phreatomagmatism explored: Tepexitl tuff ring (Eastern Mexican Volcanic Belt), J. Volcanol. Geotherm. Res. (2010), doi:10.1016/j.jvolgeores.2010.09.007

crater and flat-topped ridge surface deposits, which are considered to be the lateral equivalents of the bedded U3 deposits found at the top of the western crater rim). It is also possible that some portion of the dome remained, perhaps deflating with time, and is now covered by the crater floor deposits.

The flat-topped ridge is interpreted to be either: (1) remnants of the final, surface-level dome explosions, or (2) the result of uplift from an underlying cryptodome. If uplift occurred syn-eruption, the tuff deposits seen atop the ridge may be in their primary deposition location and are consistent with deposition of U3 deposits by low-energy wet surges produced by phreatic eruptions through saturated crater fill, likely associated with late-stage surface-level dome explosions. However, if uplift occurred post-eruption, these tuff units may represent uplifted crater fill. The massive reworked deposits found along the base of the inner crater floor (as seen in Figs. 2 and 8) are interpreted to be from syn-eruptive debris flows.

4.4. Interpretation of LOI data

Several patterns emerged from LOI data that correspond to the depositional patterns observed at Tepexitl (Fig. 11).

(1) Obsidian consistently lost a greater percentage of its volatiles by the time of quenching than stony rhyolite. This pattern is consistent with obsidian having formed in an area where volatile loss was enhanced, but quenching and eruption occurred prior to complete degassing. These trends can be explained by obsidian formation along the conduit margin or the upper portions of a rising plug, where volatile loss is highest. The degree of degassing of the vesiculating conduit interior appears to be preserved upon fragmentation.

(2) In the lower sequence, the ratio of more degassed obsidian to less degassed stony rhyolite is constant (stony rhyolite has 1.7–1.9 times the amount of magmatic water as the obsidian). This pattern can be best explained by open-system degassing, in which the gas content is proportionally higher in the middle of the conduit and lower along the edges, where the most significant degassing occurs. In other words, the amount of degassing at the margins is directly related to the volatile concentration at the center of the plug at the time of fragmentation. The implication of the data is that the depth of fragmentation of both stony rhyolite and obsidian during deposition of individual deposits of the lower sequence is roughly the same.

L2 has a notable increase in LOI in both obsidian and stony rhyolite, which means relatively less degassed magma was being fragmented and ejected. L3 data, however, indicate that the degree of degassing had sharply increased, with the lowest LOI values for obsidian of any sample. L4 and L5 fall between these two end-member extremes. These observations are consistent with a deepening of fragmentation level and/or an increase in discharge during emplacement of L2. The rapid degassing from L2 to L3 may be explained by an increased rate of shallow degassing and/or the equilibration of magma volatile release at a lower fragmentation level (rapid vesiculation post-pressure release). L4 and L5 are consistent with eruption from a stable level of fragmentation.

(3) A change in LOI pattern corresponds with the transition from the lower sequence to the upper sequence. The mirroring pattern observed for the upper sequence implies that different degrees of degassing are recorded in obsidian and stony rhyolite clasts, which indicates that the level where obsidian is quenched and the level of subsequent fragmentation are different. Early and late in the upper sequence (U1 and U3), relatively more degassed stony rhyolite was erupted simultaneously as less-degassed obsidian, consistent with shallowing of the eruptive center (Dunbar and Kyle, 1992; Lorenz et al., 2002).

This is also consistent with compositional trends — few to no lithic grains exist in deposits from early and late in the upper sequence (U1 and U3). However, the middle of the upper sequence is characterized by relatively less-degassed stony rhyolite and more degassed obsidian. This pattern could be attributed to distinct phases of nascent dome growth and subsequent explosion. It may also be caused by sampling recycled crater fill from less energetic U2 eruptions. The pumice sample is associated with U3 and has the lowest LOI values of all samples, which is consistent with surficial degassing from the outer carapace of a dome (the finely vesicular zone).

5. Conclusions

Field characteristics, componentry trends, and LOI data of Tepexitl deposits all support a change in eruptive regime from phreatomagmatic (lower sequence) to magmatic (upper sequence). Lower sequence deposits are highly deformed and fine-grained with abundant lithic clasts, and contain a repeated three-part depositional series that is consistent with highly efficient eruptions in a hot, water-rich environment. It appears that fragmentation depth migrated downward during early stages of the lower sequence, and the eruptive locus shallowed as the eruption progressed into the upper sequence. A proposed mechanism for rhyolitic phreatomagmatism is the intrusion of fluidized, saturated sediment into rapidly forming marginal cracks of a rising highly viscous plug as it invades the aquifer. Upper sequence deposits are dry and coarser-grained with few lithic clasts. Shallow dome growth and subsequent complete destruction appears to have been the final stage of eruption at Tepexitl.

Acknowledgements

Funding for this research is greatly appreciated, and was provided by: the J. William Fulbright U.S. Student Program, a U.S. Geological Survey Jack Kleinman Award, a Geological Society of America Student Research Grant, a Northern Arizona University Friday Lunch Clubbe Grant, and support through the College of Engineering and Natural Sciences and the Department of Geology awarded to Allison Austin-Erickson, and a PAPIIT IN 107907-3 (UNAM) grant awarded to Gerardo Carrasco-Núñez. Logistical support for fieldwork was provided by Centro de Geociencias (UNAM) and field colleague rockstars Chloe Bonamicci and Brian Zimmer. Many thanks to Nancy Riggs and Wendell Duffield for their support and feedback throughout the research process. Bernd Zimanowski and his team at the Physikalisch Vulkanologisches Labor in Würzburg, Germany, and Piero Dellino at the University of Bari, Italy, are gratefully acknowledged for their guidance and generosity in the use of their research facilities. Two anonymous reviewers contributed thoughtful comments that greatly enhanced the quality of this paper.

References

Adams, N.K., Houghton, B.F., Fagents, S.A., Hildreth, W., 2006. The transition from explosive to effusive eruptive regime; the example of the 1912 Novarupta eruption, Alaska. Geol. Soc. Am. Bull. 118, 620–634.

Austin-Erickson, A., Büttner, R., Dellino, P., Ort, M.H., Zimanowski, B., 2008. Phreatomagmatic explosions of rhyolitic magma: experimental and field evidence. J. Geophys. Res. 113, B11201. doi:10.1029/2008JB005731.

Bonnichsen, B., Kauffman, D.F., 1987. Physical features of rhyolite lava flows in the Snake River plain volcanic province, southwestern Idaho. Geol. Soc. Am. Spec. Pap. 212, 119–145.

Branney, M.J., Kokelaar, P., 2002. Pyroclastic density currents and the sedimentation of ignimbrites. Memoir – Geol. Soc. Lond., 27. London.

Brooker, M.R., Houghton, B.F., Wilson, C.J.N., Gamble, J.A., 1993. Pyroclastic phases of a rhyolitic dome-building eruption; Puketarata tuff ring, Taupo volcanic zone, New Zealand. Bull. Volcanol. 55 (6), 395–406.

Büttner, R., Dellino, P., Zimanowski, B., 1999. Identifying modes of magma/water interaction from the surface features of ash particles. Nature 401, 688–690.
Büttner, R., Dellino, P., La Volpe, L., Lorenz, V., Zimanowski, B., 2002. Thermohydraulic explosions in phreatomagmatic eruptions as evidenced by the comparison between pyroclasts and products from Molten Fuel Coolant Interaction experiments. J. Geophys. Res. 107 (B11), 2277–2290.
Campos Venuti, M., Rossi, P.L., 1996. Depositional facies in the Fyriplaka rhyolitic Tuff Ring, Milos Island (Cyclades, Greece). Acta Vulcanol. 8 (2), 173–190.
Cano, M., Carrasco-Núñez, G., 2008. Evolución de un cráter de explosión (maar) riolítico: Hoya de Estrada, campo volcánico Valle de Santiago, Guanajuato, México. Rev. Mex. Cienc. Geológicas 25 (3), 549–564.
Carrasco-Núñez, G., Ort, M., Romero, C., 2007. Evolution and hydrological conditions of a maar volcano (Atexcac crater, Eastern Mexico). J. Volcanol. Geotherm. Res. 159, 179–197.
Chough, S.K., Sohn, Y.K., 1990. Depositional mechanics and sequences of base surges, Songaksan tuff ring, Cheju Island, Korea. Sedimentology 37 (6), 1115–1135.
Dadd, K.A., Van Wagoner, N.A., 2002. Magma composition and viscosity as controls on peperite texture: an example from Passamaquoddy Bay, southeastern Canada. J. Volcanol. Geotherm. Res. 114, 63–80.
Dellino, P., Frazzetta, G., La Volpe, L., 1990. Wet surge deposits at La Fossa di Vulcano; depositional and eruptive mechanisms. J. Volcanol. Geotherm. Res. 43, 215–233.
Dellino, P., Isaia, R., La Volpe, L., Orsi, G., 2001. Statistical analysis of textural data from complex pyroclastic sequences: implications for fragmentation processes of the Agnano Monte Spina Tephra (4.1 ka), Phlegraean Fields, southern Italy. Bull. Volcanol. 63 (7), 443–461.
Dellino, P., Isaia, R., La Volpe, L., Orsi, G., 2004. Interaction between particles transported by fallout and surge in the deposits of Agnano-Monte Spina eruption (Campi Flegrei, southern Italy). J. Volcanol. Geotherm. Res. 133, 193–210.
Dunbar, N.W., Kyle, P.R., 1992. Volatile contents in obsidian clasts in tephra from the Taupo volcanic zone, New Zealand; implications to eruptive processes. J. Volcanol. Geotherm. Res. 49, 127–145.
Elsworth, D., Voight, B., Thompson, G., Young, S.R., 2004. Thermal-hydraulic mechanism for rainfall-triggered collapse of lava domes. Geology 32 (11), 969–972.
Erickson, A.A., 2007. Phreatomagmatic Eruptions of Rhyolitic Magma: A Case Study of Tepexitl Tuff Ring Serdán-Oriental Basin, Mexico. MS thesis, Northern Arizona University, 234 pp.
Fink, J.H., Manley, C.R., 1987. Origin of pumiceous and glassy textures in rhyolite flows and domes. Geol. Soc. Am. Spec. Pap. 212, 77–78.
Fisher, R.V., Schmincke, H.-U., 1984. Pyroclastic Rocks. Springer-Verlag, Berlin. 472 pp.
Gonnermann, H.M., Manga, M., 2005. Flow banding in obsidian; a record of evolving textural heterogeneity during magma deformation. Earth. Planet. Sci. Lett. 236 (1–2), 135–147.
Gutmann, J.T., 2002. Strombolian and effusive activity as precursors to phreatomagmatism; eruptive sequence at maars of the Pinacate volcanic field, Sonora, Mexico. J. Volcanol. Geotherm. Res. 113 (1–2), 345–356.
Heiken, G.H., Wohletz, K., 1987. Tephra deposits associated with silicic domes and lava flows. Geol. Soc. Am. Spec. Pap. 212, 55–76.
Heiken, G., Wohletz, K., Eichelberger, J., 1988. Fracture fillings and intrusive pyroclasts, Inyo Domes, California. J. Geophys. Res. 93 (B5), 4335–4350.
Hooten, J.A., Ort, M.H., 2002. Peperite as a record of early stage phreatomagmatic fragmentation processes: an example from the Hopi Buttes Volcanic Field, Navajo Nation, Arizona, USA. J Volcanol. Geotherm. Res. 114, 95–106.
Houghton, B.F., Smith, R.T., 1993. Recycling of magmatic clasts during explosive eruptions; estimating the true juvenile content of phreatomagmatic volcanic deposits. Bull. Volcanol. 55 (6), 414–420.
Houghton, B.F., Wilson, C.J.N., Weaver, S.D., 1987. The Opo Bay tuff cone, Mayor Island; interaction between rising gas-poor pantelleritic magma and external water. NZ Geol. Surv. 18, 79–85.
Houghton, B.F., Wilson, C.J.N., Smith, I.E.M., 1999. Shallow-seated controls on styles of explosive basaltic volcanism: a case study from New Zealand. J. Volcanol. Geotherm. Res. 91, 97–120.
Houghton, B.F., Wilson, C.J.N., Pyle, D.M., 2000. Pyroclastic fall deposits. In: Sigurdsson, H. (Ed.), Encyclopedia of Volcanoes. Academic Press, San Diego, pp. 555–570.
Ichihara, M., Rittell, D., Sturtevant, B., 2002. Fragmentation of a porous viscoelastic material; implications to magma fragmentation. J. Geophys. Res. 107 (B10), 1–9.
Kokelaar, B., 1982. Fluidization of wet sediments during the emplacement and cooling of various igneous bodies. J. Geol. Soc. Lond. 139 (1), 21–33.
Lorenz, V., Haneke, J., 2004. Relationship between diatremes, dykes, sills, laccoliths, intrusive extrusive domes, lava flows, and tephra deposits with unconsolidated water-saturated sediments in the late Variscan intermontane Saar-Nahe Basin, SW Germany. Geol. Soc. Spec. Publ. 234, 75–124.
Lorenz, V., 1986. On the growth of maars and diatremes and its relevance to the formation of tuff rings. Bull Volc. 48 (5), 265–274.
Lorenz, V., Zimanowski, B., Büttner, R., 2002. On the formation of deep-seated subterranean peperite-like magma-sediment mixtures. J. Volcanol. Geotherm. Res. 114, 107–118.
Manley, C.R., Fink, J.H., 1987. Internal textures of hyalite flows as revealed by research drilling. Geology 15 (6), 549–552.
Mastin, L.G., 1994. Explosive tephra emissions at Mount St. Helens, 1989–1991: the violent escape of magmatic gas following storms? Geol. Soc. Am. Bull. 106, 175–185.
Mastin, L.G., 2007. Generation of fine hydromagmatic ash by growth and disintegration of glassy rinds. J. Geophys. Res. 112, B02203. doi:10.1029/2005JB003883.
McPhie, J., Doyle, M., Allen, R., 1993. Volcanic Textures: a Guide to the Interpretation of Textures in Volcanic Rocks. University of Tasmania, Launceston. 198 pp.
Morrissey, M., Zimanowski, B., Wohletz, K.H., Büttner, R., 2000. Phreatomagmatic fragmentation. In: Sigurdsson, H. (Ed.), Encyclopedia of Volcanoes. Academic Press, San Diego, pp. 431–446.
Ort, M.H., Carrasco-Núñez, G., 2009. Lateral vent migration during phreatomagmatic and magmatic eruptions at Tecuitlapa Maar, east-central Mexico. J. Volcanol. Geotherm. Res. 181, 67–77.
Roache, M.W., Allen, S.R., McPhie, J., 2000. Surface and subsurface facies architecture of a small hydroexplosive, rhyolitic centre in the Mesoproterozoic Gawler Range Volcanics, South Australia. J. Volcanol. Geotherm. Res. 104, 237–259.
Rust, A.C., Cashman, K.V., Wallace, P.J., 2004. Magma degassing buffered by vapor flow through brecciated conduit margins. Geology 32 (4), 349–352.
Sheridan, M.F., Barberi, F., 1983. Explosive Volcanism. Elsevier, Amsterdam. 490 pp.
Sheridan, M.F., Updike, R.G., 1975. Sugarloaf Mountain Tephra; a Pleistocene rhyolitic deposit of base-surge origin in northern Arizona. Geol. Soc. Am. 86 (4), 571–581.
Sheridan, M.F., Wohletz, K.H., Dehn, J., 1987. Discrimination of grain-size subpopulations in pyroclastic deposits. Geology 15 (4), 367–370.
Siebe, C., Verma, S.P., 1988. Major element geochemistry and tectonic setting of Las Derrumbadas rhyolitic dome, Puebla, Mexico. Chem. Erde 48 (3), 177–189.
Sieh, K., Bursik, M.I., 1986. Most recent eruption of the Mono Craters, eastern Central California. J. Geophys. Res. 91 (B12), 12,539–12,571.
Sohn, Y.K., Chough, S.K., 1992. The Ilchulbong tuff cone, Cheju Island, South Korea: depositional processes and evolution of an emergent, Surtseyan-type tuff cone. Sedimentology 39 (4), 523–544.
Sohn, Y.K., Chough, S.K., 1993. The Duo tuff cone, Cheju Island, South Korea; transformation of pyroclastic fall into debris fall and grain flow on a steep volcanic cone slope. Sedimentology 40 (4), 769–786.
Tuffen, H., Dingwell, D.B., Pinkerton, H., 2003. Repeated fracture and healing of silicic magma generate flow banding and earthquakes? Geology 31 (12), 1089–1092.
Vazquez, J.A., Ort, M.H., 2006. Facies variation of eruption units produced by the passage of single pyroclastic surge currents, Hopi Buttes volcanic field, USA. J. Volcanol. Geotherm. Res. 154, 222–236.
Wilson, C.J.N., Hildreth, W.H., 1988. Hybrid fall deposits in the Bishop Tuff, California; a novel pyroclastic depositional mechanism. Geology 26 (1), 7–10.
Wilson, C.J.N., Houghton, B.F., 2000. Pyroclast transport and deposition. In: Sigurdsson, H. (Ed.), Encyclopedia of Volcanoes. Academic Press, San Diego, pp. 545–554.
Wohletz, K.H., 1983. Mechanisms of hydrovolcanic pyroclast formation; grainsize, scanning electron microscopy, and experimental studies. J. Volcanol. Geotherm. Res. 17, 31–63.
Wohletz, K.H., 2001. Pyroclastic surges and compressible two-phase flow. In: Freundt, A., Rosi, M. (Eds.), From Magma to Tephra. El Sevier, Amsterdam, pp. 247–312.
Wohletz, K.H., Heiken, G., 1992. Volcanology and Geothermal Energy. University of California Press, Berkeley. 450 pp.
Wohletz, K.H., Sheridan, M.F., Brown, W.K., 1989. Particle size distributions and the sequential fragmentation/transport theory applied to volcanic ash. J. Geophys. Res. 94, 15703–15721.
Zimanowski, B., 1998. Phreatomagmatic explosions. In: Freundt, A., Rosi, M. (Eds.), From Magma to Tephra: Developments in Volcanology, 4. Elsevier, Amsterdam, pp. 25–54.
Zimanowski, B., Fröhlich, G., Lorenz, V., 1991. Quantitative experiments on phreatomagmatic explosions. J. Volcanol. Geotherm. Res. 48, 341–358.
Zimanowski, B., Büttner, R., Lorenz, V., Häfele, H.-G., 1997. Fragmentation of basaltic melt in the course of explosive volcanism. J. Geophys. Res. 102, 803–814.
Zimanowski, B., Wohletz, K.H., Büttner, R., Dellino, P., 2003. The volcanic ash problem. J. Volcanol. Geotherm. Res. 122, 1–5.

Please cite this article as: Austin-Erickson, A., et al., Rhyolitic phreatomagmatism explored: Tepexitl tuff ring (Eastern Mexican Volcanic Belt), J. Volcanol. Geotherm. Res. (2010), doi:10.1016/j.jvolgeores.2010.09.007